Tsunami hazard posed to New Zealand by earthquakes on the Kermadec and southern New Hebrides subduction margins.

William Power[1], Laura Wallace, Xiaoming Wang, Martin Reyners

GNS Science, 1 Fairway Drive, Avalon, Lower Hutt, PO Box 30368, New Zealand

Abbreviated title: Tsunami from Kermadec and New Hebrides Arcs

Abstract

We assess the tsunami hazard posed to New Zealand by the Kermadec and southern New Hebrides subduction margins. Neither of these subduction zones has produced tsunami large enough to cause significant damage in New Zealand over the past 150 years of well-recorded history. However, as this time frame is short compared to the recurrence interval for major tsunamigenic earthquakes on many of the Earth's subduction zones, it should not be assumed that what has been observed so far is representative of the long term. For each of these two subduction zones we present plate kinematic and fault-locking results from block modelling of earthquake slip vector data and GPS velocities. The results are used to estimate the current rates of strain accumulation on the plate interfaces where large tsunamigenic earthquakes typically occur. We also review data on the larger historical earthquakes that have occurred on these margins, as well as the Global CMT catalogue of events since 1976. Using this information we have developed a set of scenarios for large earthquakes which have been used as initial conditions for the COMCOT tsunami code to estimate the subsequent tsunami propagation in the southwest Pacific, and from these the potential impact on New Zealand has been evaluated. Our results demonstrate that there is a significant hazard posed to the Northland and Coromandel regions of New Zealand should a large earthquake (Mw >~8.5) occur on the southern or middle regions of the Kermadec Trench, and that a similarly large earthquake on the southern New Hebrides Trench has the potential to impact strongly on the far northern parts of

[1] Corresponding author. Email: w.power@gns.cri.nz , Fax: +64 4 570 4600

New Zealand close to the southern end of the submarine Three Kings Ridge. We propose logic trees for the magnitude-frequency parameters of large earthquakes originating on each trench, which are intended to form the basis for future probabilistic studies.

Key words: Tsunami, New Zealand, Kermadec Arc, New Hebrides, earthquake scenarios, logic-tree

1. Introduction

The Kermadec and southern New Hebrides subduction margins (Figure 1) have been identified as key regions for concern regarding the tsunami hazard that they may pose to northern New Zealand. Both of these subduction margins have orientations which suggest that tsunami energy may be preferentially directed towards northern New Zealand following large earthquakes. However the historical data on these sources is limited, the record of large tsunamigenic earthquakes is only complete over approximately the last century, and accurate instrumental data only exists for the last 40 years. As these time frames are so short we must look to other sources of information to help estimate the tsunami hazard posed by these subduction margins.

Figure 1

Within this paper we use available seismic and geodetic data to better understand the rates of convergence and degree of interseismic coupling (where possible) at these subduction zones, and use this information to develop scenario earthquakes. The tsunami arising from these scenario events are then numerically modelled so that the potential impacts on the New Zealand coast can be assessed. In addition we develop a probabilistic model for these sources using a logic tree framework, as an initial step towards development of a fully probabilistic hazard model. We compare our results with previous modelling of tsunami originating from the southern part of the Kermadec subduction zone by WALTERS ET AL. (2006).

2. Tectonic Setting

2.1 Tectonic setting of the Kermadec Trench

The Tonga/Kermadec Trench accommodates westward subduction of the Pacific Plate beneath the active Tonga/Kermadec volcanic arc (Figure 1). Since ~5 Ma-present back-arc extension of the overriding plate has occurred along the Havre Trough (PELLETIER AND LOUAT, 1989, WRIGHT, 1993, DELTEIL ET AL., 2002) and Lau Basin (LAWVER ET AL. 1976, WEISSEL 1977, PARSON AND HAWKINS, 1994). Although the Kermadec Trench has produced two subduction thrust events of Mw ~8 in historical times (see discussion in Section 3.3), its capacity for producing earthquakes with a high tsunami hazard is not well-known. In Section 3.1 we demonstrate that GPS data from a site on Raoul Island (in the Kermadec Islands; Figure 1) suggests that the Kermadec Trench is undergoing strong interseismic coupling, possibly down to depths of ~30 km. This suggests that the Kermadec Trench may be capable of producing Mw >8.0 events.

Due to the short historical record of seismicity on the Kermadec Trench (less than ~100 years), we must use additional means to assess the likely size and recurrence intervals of earthquakes on the subduction thrust, such as long-term convergence rates and estimates of the likely rupture segments at the Kermadec Trench .

2.2 Tectonic setting of the New Hebrides Trench

Vanuatu straddles the Australia–Pacific plate boundary zone between the Tonga-Fiji region and New Guinea (Figure 1). The major tectonic features in this region are the New Hebrides Trench where the Australian plate subducts northeastward beneath Vanuatu, and a complex series of rifts and transforms in the North Fiji Basin (NFB). GPS velocities indicate that rapid clockwise rotation of the New Hebrides Arc is the primary tectonic control on the kinematics of back-arc deformation in the NFB, particularly in areas of active rifting in the Erromango and Futuna Troughs (CALMANT ET AL., 2003; PELLETIER ET AL., 1998).

It is unclear where the southeastern termination of active subduction at the New Hebrides Trench occurs but, based on seismicity, subduction is likely to terminate

somewhere between 169°E and 174°E. Defining where active subduction is ongoing at the southern New Hebrides Trench is key to assessing the tsunami hazard posed by earthquakes on the New Hebrides subduction zone to New Zealand. Large subduction thrust earthquakes on the east-west trending portion of the southern New Hebrides subduction margin (between 169°E and 174°E) could trigger tsunami that impact New Zealand coastlines. GPS data from the Matthew and Hunter Islands (Figure 1) indicate that up to 5 cm/yr of convergence is occurring on the east-west striking portion of the southern New Hebrides Trench (Section 4.1; CALMANT ET AL., 2003), suggesting that active subduction does occur on this segment of the New Hebrides Trench, at least as far east as 172°E. In Section 4.1 we demonstrate that elastic block modelling of available GPS velocities, earthquake slip vectors, transform orientations and sea floor spreading rates suggest convergence rates of 47-48 mm/yr between 170.5°E and 174°E. Earthquake slip vector and seafloor spreading data from the North Fiji Basin suggest that the Matthew Hunter Fracture Zone becomes dominated by strike-slip deformation east of 174°E.

2. Methods

For each of the two source regions, we selected scenario earthquake source events and used these as the basis for numerical tsunami modelling to the New Zealand coastline. The selection of scenario events was based on analysis of large historical earthquakes, moment tensor solutions since 1976, considerations of the tectonic setting and interpretation of regional GPS velocities and other kinematic data. Once scenario events were chosen the COMCOT tsunami model was used to follow propagation of the waves to the coast, and the results interpreted in terms of the threat posed in these scenarios.

The majority of this paper is split into two parts that focus separately on each of the source regions. However major elements of the analysis apply techniques that are common to both regions, namely the elastic block modelling which uses GPS velocities to estimate long-term convergence rates at the trench and interseismic coupling on the subduction interfaces, and the numerical tsunami propagation modelling method that is used to estimate the propagation of the tsunami from the

earthquake source to the New Zealand shoreline. These methods, and the data used to apply them, are described in the following sections.

2.1 Elastic block model for the Kermadec and Vanuatu regions

In order to understand the kinematics of tectonic blocks within the New Hebrides and Kermadec regions and to estimate the rates and nature of strain accumulation along the New Hebrides and Kermadec subduction thrusts, we employ a modeling approach that simultaneously inverts for the poles and rates of rotation of elastic, spherical blocks and locking on block-bounding faults that give the best possible fit to GPS velocities, earthquake slip vectors, transform orientations, and fault slip rate estimates. We use a program called DEFNODE described in McCAFFREY (2002) that applies simulated annealing to downhill simplex minimization (PRESS ET AL., 1989) to solve for the poles and fault locking parameters. Data misfit, determined using the reduced chi-squared statistic (X_n^2), is minimized. Surface deformation due to slip on faults in the area is calculated using an elastic, half-space dislocation model (OKADA, 1985).

Using DEFNODE we simultaneously invert GPS velocities and the earthquake slip vector and spreading rate data discussed below for the poles and rates of rotation of ten distinct tectonic blocks and the degree of interseismic coupling on the Kermadec, Tonga, and New Hebrides Trenches. We define our block boundaries based on the digital plate boundary dataset of BIRD (2003). The geometry of the Kermadec/Tonga subduction interface is based on data from BONNARDOT ET AL. (2007), and the New Hebrides subduction interface geometry we use is similar to that used for developing the Southern New Hebrides source models (see discussion of this later in the paper).

2.1.1 Data used in inversion for block rotation and fault locking in the southwest Pacific

The campaign GPS data from Raoul Island (in the Kermadec Islands) includes data collected during occupations in 1996, 1997, 2000, 2004, 2007, and 2009. Each of the campaign occupations at Raoul consisted of 3 or more consecutive 24 hour sessions. We processed the Raoul Island GPS data using GAMIT/GLOBK software (KING AND BOCK, 2002; HERRING, 2001) in combination with GPS data from several global International GPS Service (IGS) sites and a number of sites in the southwest Pacific region (including Vanuatu and Fiji) operated as part of the Southwest Pacific Sea

Level and Climate Monitoring Project (http://www.ga.gov.au/geodesy/slm/spslcmp/). The procedure used in this type of analysis has been reviewed extensively in FEIGL ET AL. (1993), HERRING ET AL. (1990), TREGONING ET AL. (1998), and MCCLUSKY ET AL. (2000). For the first stage of the GAMIT processing, we estimate station coordinates, the zenith delay of the atmosphere at each station, and orbital and earth orientation parameters (EOP's) using doubly-differenced GPS phase observations. In order to calculate site positions and velocities in a consistent reference frame (ITRF2000; ALTAMIMI ET AL., 2002), we use a loosely constrained solution (EOP's, orbital parameters, and coordinates and their covariances) from GAMIT, and loosely constrained solutions (performed by Scripps Orbit and Permanent Array Center) from the global IGS network. These loosely constrained solutions are combined in GLOBK (a Kalman filter) where we estimate a rotation and translation of each solution into the ITRF2000 reference frame for each day; we place tight constraints on the ITRF2000 positions of most of the core IGS sites in order to align the sites in our network with ITRF2000. The site velocities are estimated by a linear fit to the timeseries of daily site positions.

To better constrain Pacific/Australian Plate kinematics in our inversion we also use published velocities of GPS sites on the Pacific and Australian Plates from BEAVAN ET AL. (2002). We use velocities from CALMANT ET AL. (2003) for the Vanuatu/New Hebrides region, and data from BEVIS ET AL. (1995) for the Tonga Arc and Fiji.

To constrain relative plate kinematics in the region of the Kermadec Trench, we use 378 earthquake slip vectors from shallow (< 40 km depth) reverse faulting events on the Kermadec Trench and 442 events on the Tonga Trench (earthquake data from the Global CMT catalogue; DZIEWONSKI AND WOODHOUSE, 1983; Figure 2). We use transform orientations in the Havre Trough from DELTEIL ET AL. (2002) and t-axis orientations from earthquakes in the Havre Trough from PELLETIER AND LOUAT (1989) to provide additional information on kinematics between the Kermadec Arc and Australian Plate.

Figure 2

For the New Hebrides and north Fiji Basin region, we use earthquake slip vectors (data from the Global CMT catalogue; DZIEWONSKI AND WOODHOUSE, 1983) from 241 shallow earthquakes (< 40 km depth) near the major tectonic boundaries in the region, including the New Hebrides Trench, and various rifting and transform boundaries within the North Fiji Basin (Figure 2). Sea floor spreading rates on the various spreading centers in the North Fiji Basin are also used to help constrain the kinematics of deformation (seafloor spreading data compiled from various studies summarised in PELLETIER ET AL., 1998)

2.2 Tsunami modeling method

Tsunami hazards to New Zealand are evaluated via an in-house tsunami model - COMCOT (Cornell Multi-grid Coupled Tsunami model). COMCOT adopts a modified leap-frog finite difference scheme to solve (both linear and nonlinear) shallow water equations in a staggered nested grid system. The model is capable of simulating the propagation and the subsequent runup and inundation of tsunami generated from either local or distant sources. This model has been systematically validated against analytical solutions, experimental studies and benchmark problems in the 3rd International Long Wave Workshop in 2003 (LIU, CHO AND FUJIMA, 1994; LIU ET AL., 1995; CHO, 1995; WANG ET AL., 2008). It has been widely used to investigate historical tsunami events, such as the 1960 Chilean tsunami, the 1992 Flores Islands (Indonesia) tsunami (LIU ET AL., 1994, 1995) and more recently, the 2004 Indian Ocean tsunami (WANG AND LIU, 2006, 2007; WIJETUNGE ET AL., 2008).

With the implementation of two-way nested grid coupling, COMCOT simultaneously calculates the tsunami propagation in ocean with a relatively larger grid resolution and inundation process in the targeted coastal zones with a finer grid resolution via a two-way coupling algorithm. To simulate the onshore flooding, a moving boundary scheme described by CHO (1995) was employed, in which the "shoreline" is defined as the interface between a wet grid and its neighbouring dry grids.

In this study, three levels of bathymetric/topographic data resolution were implemented to model the tsunami propagation and runup. The first-level grids cover the entire region of New Zealand, Kermadec-Tonga trench and New Hebrides trench,

ranging from 145°E to 190°E in longitude and from 50°S to 4°S in latitude, with spatial resolution of 2 arc-minutes (grid 01 in Figure 3). The second-level grid covers the entirety of New Zealand, including the Chatham Islands, with a spatial resolution of 30 arc-seconds (grid 02 in Figure 3). The third-level grids include two sub-grid regions (grid 03 and 04 in Figure 3) covering the regions of Northland, Auckland and Waikato with spatial resolution of 10 arc-seconds in order to obtain more detailed results around these high-risk regions. This high resolution bathymetric and topographical data was derived from the National Geophysical Data Center ETOPO2 database, the GEBCO_08 30 arc-second database and from Land Information New Zealand nautical charts. Linear shallow water equations are applied in the first- and second-level grids to model the propagation of tsunami in deep water. In the third level grids, nonlinear shallow water equations are implemented to simulate runup and inundation.

Figure 3

In this paper, scenario earthquakes are constructed along the Kermadec and New Hebrides subduction trenches. The seafloor displacement caused by an earthquake is computed via OKADA's (1985) elastic finite fault plane model. And it is further assumed that water surface follows the seafloor motion instantaneously, which becomes the source of the tsunami. Results from the tsunami modelling are presented with reference to the locations shown in Figure 4.

Figure 4

3. Kermadec Arc

3.1 Results from best-fitting elastic block model

In our best-fitting elastic-block model (Section 2.1) for the Kermadec Arc, we obtain an excellent fit to earthquake slip vectors and GPS velocities, yielding an $X_n^2 = 2.19$. The long-term convergence rate at the Kermadec Trench is 53 mm/yr near 35°S and increases northward to ~90 mm/yr near 25°S (Figure 5). Back-arc rifting rates in the

Havre Trough are ~13 mm/yr near 35°S and increase to 25 mm/yr near 25°S. The oblique portion (right lateral sense) of Havre Trough rifting accommodates most of the margin-parallel component of Pacific/Australia relative motion. The most intriguing result for the Kermadecs portion of the study area is the strong interseismic locking on the Kermadec Trench that is required to fit the campaign GPS site velocity at Raoul Island (Figure 5). This coupling is required by the kinematic model to fit the westward motion of Raoul Island with respect to the Australian Plate, while simultaneously satisfying the kinematic constraints of active back-arc rifting in the Havre Trough. In our best-fitting inversion, interseismic coupling occurs down to ~30 km on the subduction interface in the region of the Kermadec Islands. Although strong, deep interseismic coupling may occur on the Kermadec Trench in the vicinity of Raoul Island, it is not possible to constrain the degree of coupling on the interface further north and south along strike of Raoul Island, as this is the only landmass in the Kermadec Arc for which we have GPS data.

Figure 5

3.2 Geometry of the plate interface

The Kermadec Trench is the surface expression of the subduction interface between the Pacific Plate and the Australian Plate, located between 38°S and 25-26°S. The northern boundary of the Kermadec Trench is defined by the intersection of the Louisville Seamount Chain with the Tonga/Kermadec Trench. Most of the Kermadec Trench is over 8 km deep, although the water depths near the northern and southern ends are shallower. The depth at the southern end is around 4 km, due to the subduction of the over-thickened Hikurangi plateau beneath New Zealand's North Island. At the northeastern end, subduction of the Louisville Seamount Chain produces a noticeable deformation and shallowing of the trench, decreasing the depth to about 5-6 km below sea level.

The geometry of the plate interface plays an important role in determining the initial conditions for tsunami modeling, including the strike, dip and depth of the plate interface where an earthquake is initiated. The geometry of the Kermadec plate

interface has been revealed via seismic reflection surveys and seismicity analysis. Down-dip depth transects from these studies have been used in this paper to reconstruct the geometry of the Kermadec plate interface.

Using the seismic reflection data collected during the cruises of the MANGO project (Marine Geoscientific Investigations on the Input and Output of the Kermadec Subduction zone), SCHERWATH ET AL. (2008) determined crustal structure along four marine transects through the Hikurangi-Kermadec subduction zone between 29.0°S and 38.0°S. Their results show that at the southern end of the Kermadec Trench around 38°S-37°S, the Hikurangi Plateau subducts beneath the North Island of New Zealand at a low angle, dipping about 4-6° between 4 km and 13 km depth, and increasing to 25° dip at depths >13km. Further to the north along the trench, the dip angle increases to 6° from 8 km - 15 km between 35°S-33°S, and dips 9° from 8km - 12 km depth near 29.5°S.

We have also developed a down-dip section of seismicity through Raoul Island (near 30°S) using earthquakes from the high quality seismicity catalogue of ENGDAHL ET AL. (1998), as relocated by NICHOLSON (2006) using the empirical travel time method. We used earthquakes within 50 km of the section. The Backarc crustal thickness is reasonably well-defined by these data at about 33 km. The trench here is ~8 km deep and the dip angle of the plate interface is 12° between 8km and 20 km depth, and 18° between 20 and 33 km depth.

At the northern end of the Kermadec Trench, BONNARDOT ET AL. (2007) computed a down-dip cross section through the junction with the Louisville Seamount Chain, using Bossu's method (BOSSU, 2000) with data from the Engdahl catalog (ENGDAHL ET AL., 1998). The transect profile gives a dip angle of ~18° for < 50km depth and 58° for > 50km depth.

The down-dip profiles of these sections are summarized in Table 1, and these were used as constraints on the geometry of the Kermadec plate interface.

Table 1 Down-dip transects through the Kermadec subduction interface

Down-dip Transect	Crossing trench at (Lon Lat)		Trench Depth	Dip angle
Mango-1 (OBS/H 01-29)	179.75	-37.80	4.00 km	4° (4-8 km); 6° (8-13 km); 25° (>13 km)
Mango-2 (OBS/H 30-59)	181.25	-35.12	7.00 km	6° (7-12 km); 15° (>12 km)
Mango-3 (OBS/H 60-89)	182.20	-33.20	8.00 km	6° (8-15 km); 14° (>15 km)
Raoul Island	183.64	-29.95	8.00 km	12° (8-20 km); 18° (20-33 km)
Mango-4 (OBS/H 90-119)	183.75	-29.40	8.00 km	9° (8–12 km); 15° (>12 km)
Bonnardot et al. (2007) - c	184.70	-26.00	6.00 km	18° (< 50 km); 58° (>50 km)

Using a relationship between the crustal thickness and volcanic centre spacing, DE RONDE ET AL. (2007) suggest a crustal thickness of 17.5 km for a volcanic centre spacing of 45 km in the back arc of the middle Kermadec Arc and a thickness of 22.5 km for a 58 km spacing in the arc front. These estimates are consistent with the refraction measurements of crustal thickness on the Kermadec Ridge by SHOR ET AL. (1971), which range from 16 km at 34.2ºS to 19 km at 33.07ºS. Together with the dip estimates, this suggests that the rupture width of earthquakes on the Kermadec subduction interface may reach up to about 100 km, if the maximum downdip limit of rupture is constrained by the forearc crustal thickness

Figure 6

With the above constraints, we have developed 100 km by 50 km "unit source" patches along the Kermadec subduction interface in order to account for the down-dip and along-strike variation of the plate interface as well as to keep a simple representation of the interface geometry for tsunami modelling (Figure 6). The technique of constructing earthquake rupture models for tsunami sources from unit sources was developed by TITOV ET AL. (1999), who studied the sensitivity of the tsunami wavefield to variations in the patch parameters. The top edges of the shallower unit patches are aligned with the deepest part of the subduction zone trench. The dip angle and depth to the top edge of each unit patch are interpolated from the down-dip transects shown in Table 1. The strike angle of each patch is determined by the local azimuth of the trench.

Table 2. Geometric description of unit source patches for the Kermadec subduction interface.

KT	Starting-pts		Ending-pts		Mid-pts		Depth*	Strike	Dip	Rake
#	Lon	Lat	Lon	Lat	Lon	Lat	Km	Deg	deg	deg
01a	179.3860	-38.1877	180.0000	-37.4280	179.6930	-37.8079	3.97	212.40	4.00	90.00
02a	180.0000	-37.4280	180.5998	-36.6770	180.2999	-37.0525	4.90	212.30	4.60	90.00
03a	180.5998	-36.6770	181.0378	-35.8477	180.8188	-36.2624	5.82	202.90	5.21	90.00
04a	181.0378	-35.8477	181.5072	-35.0342	181.2725	-35.4410	6.69	205.00	5.79	90.00
05a	181.5072	-35.0342	181.8827	-34.1893	181.6950	-34.6118	7.31	200.00	6.00	90.00
06a	181.8827	-34.1893	182.2113	-33.3288	182.0470	-33.7591	7.73	197.50	6.00	90.00
07a	182.2113	-33.3288	182.5242	-32.4683	182.3678	-32.8986	8.00	196.90	6.58	90.00
08a	182.5242	-32.4683	182.8371	-31.6078	182.6807	-32.0381	8.00	197.00	8.12	90.00
09a	182.8371	-31.6078	183.1969	-30.7629	183.0170	-31.1854	8.00	199.90	9.67	90.00
10a	183.1969	-30.7629	183.6037	-29.9337	183.4003	-30.3483	8.00	202.80	11.22	90.00
11a	183.6037	-29.9337	183.9010	-29.0732	183.7524	-29.5035	8.00	196.70	9.55	90.00
12a	183.9010	-29.0732	184.1357	-28.1970	184.0184	-28.6351	7.54	193.20	11.07	90.00
13a	184.1357	-28.1970	184.3547	-27.3208	184.2452	-27.7589	7.03	192.40	13.37	90.00
14a	184.3547	-27.3208	184.5581	-26.4447	184.4564	-26.8828	6.52	191.70	15.67	90.00

KT	Starting-pts		Ending-pts		Mid-pts		Depth*	Strike	Dip	Rake
#	Lon	Lat	Lon	Lat	Lon	Lat	Km	Degree	degree	degree
01b	178.9090	-37.9471	179.5163	-37.1886	179.2142	-37.5678	7.46	212.40	6.00	90.00
02b	179.5244	-37.1929	180.1240	-36.4336	179.8257	-36.8133	8.92	212.30	8.71	90.00
03b	180.0903	-36.5021	180.5229	-35.6746	180.3078	-36.0883	10.36	202.90	11.45	90.00
04b	180.5418	-35.6592	181.0067	-34.8451	180.7754	-35.2521	11.74	205.00	14.07	90.00
05b	180.9977	-34.8811	181.3704	-34.0369	181.1850	-34.4590	12.54	200.00	14.69	90.00
06b	181.3715	-34.0532	181.6960	-33.1964	181.5346	-33.6248	12.96	197.50	14.27	90.00
07b	181.7033	-33.1987	182.0139	-32.3391	181.8593	-32.7689	13.73	196.90	14.39	90.00
08b	182.0236	-32.3376	182.3331	-31.4786	182.1791	-31.9081	15.06	197.00	15.41	90.00
09b	182.3511	-31.4570	182.7080	-30.6123	182.5303	-31.0347	16.40	199.90	16.44	90.00
10b	182.7274	-30.5916	183.1302	-29.7635	182.9296	-30.1776	17.73	202.80	17.48	90.00
11b	183.1162	-29.8064	183.4124	-28.9460	183.2649	-29.3762	16.30	196.70	15.55	90.00
12b	183.4122	-28.9717	183.6457	-28.0971	183.5294	-28.5344	17.14	193.20	15.69	90.00
13b	183.6536	-28.1038	183.8714	-27.2264	183.7629	-27.6651	18.59	192.40	16.46	90.00
14b	183.8792	-27.2349	184.0832	-26.3553	183.9816	-26.7951	20.02	191.70	17.22	90.00

These unit patches are used to construct the subduction interface geometry for the scenario earthquakes developed in the following sections. A similar approach has also been used by PTWC for its operational tsunami early warning and forecast system (TITOV ET AL., 2005).

3.3 Kermadec Arc: Review of Historical Earthquakes

The historical record of earthquakes on the Kermadec Arc is short, and is only complete for major earthquakes (greater than about Mw 7.5) over the past century. This is primarily a consequence of the remote location and of the largely uninhabited nature of the few islands along the arc. Polynesian people did settle on the Kermadec islands in the fourteenth century, but when Europeans reached the area in the late 18th century they found no inhabitants; presumably any earlier oral history of earthquakes or tsunami was lost. Outside of the Kermadec Arc the area most likely to be affected by tsunami originating on the arc is the Northland Peninsula of New Zealand. Oral traditions and paleotsunami studies suggest that this area has indeed been subject to substantial tsunami (GOFF, 2008), but there is insufficient evidence to clearly implicate a Kermadec Arc earthquake source.

Here we review the three most significant subduction-related earthquakes in this region since the beginning of the 20th century, namely the earthquakes of 2 May 1917, 14 Jan 1976, and 20 October 1986 (Figure 5).

3.3.1 The earthquake of 2 May 1917

A substantial earthquake and subsequent tsunami occurred close to Raoul Island on the Kermadec Arc on 2 May 1917 at 29.2ºS, 177ºW. This event is sometimes confused with the June 26 1917 earthquake and tsunami in Samoa. Estimates of the earthquake magnitude are quite variable, a probable consequence of the quality and sparse distribution of instrumentation at that time. RICHTER (1958) and DUDA (1965) assigned a magnitude of 8.6 for this event. HECK (1947), IIDA ET AL. (1967) and LANDER AND LOCKRIDGE (1989) assigned a magnitude of 8; IIDA ET AL. (1967) also inferred that the earthquake was shallow.

A tsunami was observed on tide gauges in Hawaii and on the east coast of the Pacific at arrival times consistent with this source (Table 3; NGDC Database). A large run-up of 12.2 m in Samoa was reported for this event by HECK (1947), but this is most likely

a misattribution of observations relating to the June 26 Samoa earthquake (IIDA ET AL., 1967; SOLOVIEV AND GO, 1975).

COUNTRY	LOCATION	MAX WATER HEIGHT (M)	TYPE
Canada	Tofino, B.C.	.06	Gauge
USA	La Jolla, CA	Obs	Gauge
USA	San Diego, CA	0.10	Gauge
USA	San Francisco	0.10	Gauge
USA	Honolulu, Hawaii	0.30	Gauge

Table 3: Observations of the 2 May 1917 tsunami (Adapted from NGDC database).

The observed amplitudes are similar to those of the 2009 Samoa tsunami at the locations in Table 3, despite a less favourable orientation of the source for directing tsunami energy tsunami towards Hawaii and the west coast of the USA. On this basis we suggest a magnitude similar to or slightly greater than that of the Mw 8.1 2009 Samoa earthquake.

3.3.2 The earthquakes of 14 Jan 1976

A series of substantial earthquakes occurred in the Kermadec Islands region on 14 January 1976 at 28.43ºS 177.66ºW. The two largest shocks occurred at 15.56 and 16.47 (UTC), and were assessed by NEIC (2010) to have magnitudes of 7.8 and 8.0 respectively. Some damage was caused on Raoul Island, with a felt intensity estimated at VIII. The global CMT solution for the second of these shocks suggests a shallow (18km) low-angle (11°) thrust earthquake of Mw 7.9. This earthquake caused a tsunami that was widely observed in the Pacific, primarily on tide gauges, but also as observed run-ups (Table 4). Several yachts were damaged in Tutukaka harbour near Whangarei in New Zealand (Bay of Plenty Times, 15 January 1976; DOWNES, PERS COMM.; Figure 4)

COUNTRY	LOCATION	MAX WATER HEIGHT (M)	TYPE
Australia	Lord Howe I.	0.30	Gauge

Fiji	Southern Fiji	0.90	Run-up
Fiji	Suva	0.23	Gauge
Mexico	Acapulco	0.24	Gauge
Mexico	Cabo San Lucas	0.08	-
Mexico	Manzanillo	0.21	-
Mexico	Puerto Vallarta	0.14	-
Mexico	Salina Cruz	0.18	Gauge
New Zealand	Auckland	Obs	-
New Zealand	Tauranga	Obs	-
New Zealand	Tutkaka	0.2-0.75	Run-up
New Zealand	Whangarei	Obs	-
Samoa	Apia	0.07	Gauge
USA	Honolulu, HI	0.03	Gauge
USA	Kahului, HI	0.15	Gauge
American Samoa	Pago Pago	Obs	Gauge

Table 4. Observations of the 14 Jan 1976 tsunami (Adapted from NGDC database; New Zealand observations from DOWNES, PERS COMM.). These observations are believed to originate from the earthquake at 16.47 (UTC).

3.3.3 The earthquake of 20 October 1986

This earthquake was studied in detail by LUNDGREN ET AL. (1989), who interpreted that this short source-duration and high stress-drop event was caused by internal deformation within the subducting Pacific slab. NEIC assign an Ms of 8.1 and a location of 28.117°S 176.367°W; there is considerable variation in estimates of the seismic moment (LUNDGREN ET AL., 1989), the global CMT catalogue gives Mw 7.7 (Mo=4.5e27 dyn-cm), while LUNDGREN ET AL. (1989) estimate Mo=8.5e27 dyn-cm corresponding to Mw ~7.9. A subsequent tsunami was instrumentally observed but was everywhere small, consistent with an intra-slab mechanism (Table 5).

COUNTRY	LOCATION	MAX WATER HEIGHT (M)	TYPE
French Polynesia	Papeete	0.07	Gauge

French Polynesia	Rapa	0.10	-
USA	Hilo, HI	0.11	Gauge
USA	Honolulu, HI	0.07	Gauge
USA	Honuapo, HI	0.07	Gauge
USA	Kahului, HI	0.08	Gauge
USA	Kailua-Kona	0.04	Gauge
American Samoa	Pago Pago	0.05	Gauge

Table 5: Observations of the 20 October 1986 tsunami (Adapted from NGDC database).

3.4 Magnitude frequency of seismicity data 1976-2009

The Global CMT catalog was searched for thrust events (T-axis plunge between 45 and 90 degrees) on the Kermadec Arc from 1976 to 2009 inclusive. The primary search area was between 26-38 °S and 174-180 °W, and this search yielded 544 events. South of 34°S the search area was extended to 178°E, which added an additional 4 events.

The total seismic moment release in these events was $1.22*10^{28}$ dyn-cm. Assuming a down-dip width of 100km this is equivalent to an average annual slip of 8.8 mm on the subduction interface that is released in such events, or just over 12% of the plate convergence rate. This does not tell us what proportion of the remaining slip is released aseismically, or what proportion is accumulated as strain to be released in larger events occurring on longer timeframes.

A plot of the cumulative number of events greater than or equal to a given magnitude over this 34-year period is shown in Figure 7. Below Mw 5.5 the catalog shows signs of incompleteness, and above Mw 6.5 there are insufficient events to produce reliable statistics. The trendline shown, based on all available datapoints implies a b-value of 1.12.

Figure 7

We consider the extrapolation of magnitude frequency curves to significantly larger events to be of very limited reliability (SCHWARTZ AND COPPERSMITH, 1984), especially where there is a change in earthquake scaling characteristics, as happens here once we enter the domain where the typical earthquake width reaches the full down-dip extent of the coupled subduction interface (SCHOLZ, 1982; HANKS AND BAKUN, 2002; ROMANOWICZ, 1992, 1994; POWER ET AL., 2007). However, if we extrapolate the trendline to estimate the frequency of events greater than or equal to Mw 8.0 we find that such events are expected approximately once per century; in comparison we find two probable events of this magnitude or greater in the historical record for the last century (see Section 3.3).

3.5 Tsunami scenario results

In order to develop tsunami scenarios for the Kermadec subduction zone it is necessary to investigate the segmentation of the trench according to variations in its physical properties. While we have identified segments according to such changes we note that on the relatively homogeneous Kermadec Trench these changes are probably insufficient to act as impassable barriers to rupture – historic earthquakes in other parts of the world have ruptured across areas with greater heterogeneity (SUBARYA, 2006; KENNET AND CUMMINS, 2005; OKAL ET AL., 2006; TAYLOR ET AL., 2008). Even at the southern and northern ends of the trench we cannot be certain that a rupture will not cross into or out of the Hikurangi subduction zone or the Tonga Trench, though the changes there are much more distinct than those along the Kermadec Trench.

At the southern end of the trench, between approximately 35-38ºS, the subducting crust is relatively thick as the over-thickened Hikurangi plateau is subducted. The trench here is relatively shallow (about 4 km deep), and the initial dip angle is relatively shallow (4-6º). In this region there is ~1 km of sediment entering the trench, while the Kermadec Trench further north is sediment-starved. Here there are also sedimentary basins in the back-arc. We define this region as segment A.

In the middle region of the trench, between approximately 35-31ºS, the subducting crust is thin, and the dip angle of the shallow part of the plate interface is intermediate

(6-10º), the sedimentation rate is low here, and the trench is very deep at ~8 km. We define this region as segment B.

At the northern end of the trench, between approximately 31-25ºS, the subducting plate dips quite steeply (10-20º) even on the shallow part of the plate interface. The trench becomes steadily shallower from south (8 km deep) to north (5 km deep), and the bathymetry above the plate interface is shallower than in segment B. We define this region as segment C. The intersection of the Louisville Seamount Chain with the trench (Figure 1) marks the northern edge of this segment.

We also develop a scenario in which the entire Kermadec subduction interface ruptures. While we regard this as an event which is unlikely to ever take place we also find that it cannot be ruled out on simple empirical grounds because of the short recorded history (Appendix I; McCaffrey 2007). Modelling such an unlikely scenario is nonetheless useful as it assists in the filtering of possible explanations for paleotsunami records. It is also helpful to understand the potential impact of such an event in case it were to occur. (Travel times to northern New Zealand are sufficiently long that some advance warning may be possible).

Scenario earthquakes have therefore been constructed to rupture the southern (Segment A), the middle (Segment B), the upper (Segment C) and the entire Kermadec subduction interface (Segment A+B+C), respectively. The rupture surface of a scenario earthquake is composed of a set of unit patches which account for the variation in dip and strike of the subduction interface. Detailed information on the scenario earthquakes is given in Table 6, and the segments are illustrated in Figure 6.

Table 6 Scenario earthquakes along Kermadec subduction zone

Scenario	Segment	Unit Patch	Length	Width	Slip	Magnitude
1	A	01a-03a, 01b-03b	300 km	100 km	5.0 m	Mw 8.5
2	B	04a-09a, 04b-09b	600 km	100 km	10.0 m	Mw 8.9
3	C	10a-14a, 10b-14b	500 km	100 km	8.0 m	Mw 8.8

4	A+B+C	01a-14a, 01b-14b	1400 km	100 km	22.0 m	Mw 9.4

The scaling relationship used to estimate the slip for a given rupture length is based on adapting that of POWER ET AL. (2007) to a 100 km rupture width. This assumes that the scaling relations of ABE (1975) hold for magnitudes up to that at which the rupture width extends for the full width of the fault plane (to the brittle ductile boundary where fault-locking no longer occurs). Above this magnitude it is assumed that the displacement continues to scale proportionately with the fault length; this is known as the L-model (SCHOLZ, 1982; HANKS AND BAKUN, 2002). POWER ET AL. (2007) found this model to give a better match to large historical earthquakes on the South American plate interface than the alternative W-model (ROMANCOWICZ, 1992, 1994).

In Scenario 1, an earthquake with a magnitude Mw 8.5 is assumed to rupture the southern part of the Kermadec subduction zone (Segment A) ~300 km along the trench from offshore Raukumara Peninsula of New Zealand's North Island to the north end of the Hikurangi Plateau at about 35.8°S.

In Scenario 2, the earthquake is assumed to rupture the middle portion of the Kermadec Trench with a magnitude of Mw 8.9. The rupture area is 600 km in length and 100 km in width (Segment B).

In Scenario 3, an Mw 8.8 earthquake is assumed to rupture the upper portion of the Kermadec interface from about 30.8°S to the junction with Louisville Seamount Chain (Segment C), with a rupture length of 500km.

For the most severe scenario, Scenario 4, it is assumed that an earthquake is capable of rupturing the entire subduction zone (Segments A+B+C) with magnitude Mw 9.4, which is comparable to the 2004 Sumatra earthquake in both rupture area and magnitude. We consider that such a scenario is unlikely to ever occur (12% weighting in the logic-tree of Appendix I), but we include this scenario as the possibility of rupture of the entire trench cannot be ruled out empirically (MCCAFFREY, 2007).

For each scenario, 10-hours of wave evolution have been modelled in order to obtain the maximum wave amplitude on- and off-shore, and hence evaluate the tsunami hazard to New Zealand, particularly to the coasts of North Island.

Numerical results (plotted in Figures 8-11) show that tsunami generated from the southern and/or middle segments of the Kermadec subduction zone impose a larger hazard to the coast of New Zealand than tsunami generated along the northern Kermadec Trench. For tsunami generated by the northern Kermadec rupture scenario, the majority of energy travels towards the open Pacific, as well as through the South Fiji Basin to the northwest toward Norfolk Island and New Caledonia (Figure 10). In contrast, if the southern and/or middle segments of Kermadec plate interface are ruptured, refraction effects due to the sloping continental shelf of North Island will gradually bend tsunami wave rays onshore, and thus much more energy will be directed toward the coasts of the Northland and Auckland regions (Figures 8,9). Diffracted waves around the northwestern tip of North Island will also affect the southwestern coast of the Aupouri Peninsula and Ahipara Bay on the Northland coast (location shown on Figure 3), with water levels comparable to those along its northeastern coast.

A zone with exceptionally high water levels is also identified at about 50-60 km off the southwestern coast of Northland's Aupouri Peninsula for tsunami generated from the Kermadec plate interface, especially from its middle and/or southern part (Figures 8, 9, 11). Detailed modeling shows that the exceptional height of water level offshore is created by the merging of diffracted waves through the gap between Great Island (the largest of the Three Kings Islands) and the northwestern tip of Northland, and those through the South Norfolk Basin and Reinga Basin outside Great Island (locations shown on Figure 3). Although further away from the coast of Northland, the fast-travelling diffracted waves through Reinga Basin are able to catch up with those slow-travelling waves through the gap between Great Island and Northland. The two wave chains converge along a course over 50 km offshore, resulting in greatly raised water levels, and finally hit the coast near Tauroa Point, causing tsunami waves significantly higher than in neighbouring regions.

As the modelled earthquake rupture location is moved from north to south along the Kermadec subduction zone, the areas impacted by larger wave amplitudes also shift south along the northeast coast of North Island, from the coast of Northland south to the coasts of Auckland, Waikato, Bay of Plenty and Gisborne.

Figure 8

For earthquake Scenario 1 (Segment A; Figure 8), water levels 3-5 m above mean sea level are found along the northeastern coasts of Northland and the Auckland region as well as the coasts of Gisborne and the Bay of Plenty. Over 10.0 meter wave amplitudes are observed on the northeastern coasts of Great Barrier Island. Water level increases of 1.0-3.0 meters are widely found along the southwestern coast of Northland.

Figure 9

In Scenario 2, in which a tsunami is generated by an Mw 8.9 earthquake rupturing the middle portion of Kermadec plate interface (Segment B; Figure 9), water levels are increased by up to 5.0-7.0 meters above mean sea level at many places along the northeastern coast of Northland. Significant water level increase, up to 3.0-5.0 meters, is also present along its southwestern coast of the Aupouri Peninsula.

Figure 10

In Scenario 3 (Segment C; Figure 10), wave amplitudes of less than 1.5 meters are observed along most parts of the northeastern coast of North Island from Gisborne to Northland. At the outermost tips of the Raukumara and Northland Peninsulas wave amplitudes may reach up to around 2.0 m. Along the northeastern coast of Great Barrier Island offshore Auckland, wave levels are raised by 2.0 to 3.0 m.

Figure 11

In the worst scenario, the entire Kermadec subduction interface is ruptured by an Mw 9.4 earthquake (Segment A+B+C; Figure 11). Numerical simulation illustrates that an earthquake of this size will trigger tsunami causing tremendous damage throughout the coastal areas between Gisborne and Northland. Along the coasts of the Raukumara Peninsula and the Bay of Plenty, wave amplitudes around 5-10 m above the normal level are widely observed. On many parts of the northeastern coasts of Great Barrier Island and Northland, tsunami runup heights are about 15-20 m above the normal level. Tsunami waves of over 10 m amplitude also strike the southwestern coast of the Aupouri Peninsula and Ahipara Bay in northern Northland.

4. Southern New Hebrides

4.1 Results from best-fitting elastic block model

In our best-fitting model for the Vanuatu region (Figure 12), we obtain 46-48 mm/yr convergence on the southern New Hebrides Trench, south of Matthew and Hunter Islands (Figure 1). Although our inversion results require minimal interseismic coupling on this portion of the New Hebrides Trench, it is not possible to constrain the degree of interseismic coupling on the southern New Hebrides Trench due to the lack of available GPS data to constrain arc-perpendicular contractional strain combined with minimal prior knowledge of the kinematics and rates of deformation in the back-arc region to the north of Matthew and Hunter Islands. We suggest that convergence on the southeastern-most portion of the New Hebrides Trench terminates near 174E, based on the shift from reverse fault dominated focal mechanisms on that boundary to left-lateral strike-slip dominated earthquakes, as well as the intersection of the Central Spreading Ridge (AUZENDE ET AL., 1994) with the southern New Hebrides Trench/Matthew Hunter Fracture zone at this point.

Figure 12

4.2 Geometry of the plate interface

To reveal the geometry of the southern New Hebrides plate interface, we have developed three down-dip seismicity cross-sections for three segments of the southern New Hebrides subduction zone (see Table 7), by using the high quality seismicity catalogue of ENGDAHL ET AL. (1998), as relocated by NICHOLSON (2006) using the empirical travel time method.

Table 7 Down-dip transects of seismicity for the three New Hebrides segments

Segment	Top Depth	Base Depth	Dip Angle	Crossing trench at (lon, lat)
Western	5 km	30 km	25°	(169.817°E,22.155°S)
Middle	5 km	30 km	25°	(171.555°E,23.036°S)
Eastern	5 km	30 km	33°	(173.238°E,23.024°S)

For the western segment, the depth section includes events from 240 km along strike. Backarc crustal thickness based on seismicity is about 30 km. Average dip of the plate interface from the trench is 25º between 5km and 30 km depth.

For the middle segment, the depth section includes events from the eastern half of the segment, 90 km along strike. Backarc crustal thickness based on seismicity is poorly constrained and estimated at ~30 km. Such a crustal thickness is consistent with the ~29 km estimated from subaerial volcano spacing (Hunter Island to Matthew Island). The average dip of the plate interface between the trench at 5 km depth and the base of the crust at 30 km is 25º.

For the eastern segment, the depth section includes events from the eastern 110 km of the segment along strike. Backarc crustal thickness based on seismicity is about 30 km and the average dip of the plate interface from the trench at 5 km depth and the base of the crust at 30 km is 33º.

Figure 13

With these estimates of dip angles and crust thickness, the rupture width may reach up to 60km in an earthquake in the southern New Hebrides subduction zone. Using these

constraints, unit patches with dimensions of 100 km by 60 km were constructed to reflect the geometric variation of the plate interface (Figure 13). The top edges of the unit patches are aligned with the deepest portion of the trench and extend down-dip. The dip angle and depth to the top edge of each unit patch are interpolated from the down-dip transects shown in Table 7. The strike angle of each unit patch is determined by the local trench orientation. The parameters of the unit patch geometry along the southern New Hebrides subduction zone are summarized in Table 8.

Table 8 Parameters of unit patches along southern New Hebrides subduction zone

NH	Starting-pts		Ending-pts		Mid-pts		Depth*	Strike	Dip	Rake
#	Lon	Lat	Lon	Lat	Lon	Lat	Km	deg	degree	degree
01	174.9929	-22.3838	174.1330	-22.8069	174.5630	-22.5954	5.00	241.78	33.00	90.00
02	174.1330	-22.8069	173.1873	-23.0260	173.6602	-22.9165	5.00	255.70	32.35	90.00
03	173.1873	-23.0260	172.2160	-23.1194	172.7017	-23.0727	5.00	263.85	30.45	90.00
04	172.2160	-23.1194	171.2446	-23.0727	171.7303	-23.0961	5.00	272.80	25.84	90.00
05	171.2446	-23.0727	170.3667	-22.6710	170.8057	-22.8719	5.00	296.24	25.00	90.00
06	170.3667	-22.6710	169.6102	-22.1013	169.9885	-22.3862	5.00	309.01	25.00	90.00
07	169.6102	-22.1013	168.9750	-21.3728	169.2926	-21.7371	5.00	320.74	25.00	90.00

4.3 Southern New Hebrides Arc: Review of Historical Earthquakes

The historical record of earthquakes on the Southern New Hebrides is short, and complete for major earthquakes (Mw >~7.5) only over the past century. This is primarily a consequence of the remote location, the largely uninhabited nature of the few islands on the eastern part of the arc, and the lack of surviving oral history accounts from the pre-colonisation cultures on the islands in the region of interest.

Here we review the most significant subduction-related earthquake in this region, namely the earthquake of 9 August 1901 (Figure 12).

4.3.1 The earthquake of 9 August 1901

A substantial earthquake and subsequent tsunami occurred close to the Loyalty Islands on 9 August 1901. The NGDC SIGNIFICANT EARTHQUAKE DATABASE (2010) gives the location as 22°S 170°E. The magnitude of this event is estimated as M 8.4 by DUDA (1965), and LOMINTZ (1974), and M 7.9 by RICHTER (1958) and GUTENBERG (1956).

The SYDNEY MORNING HERALD (1901a) reported that several lives were lost on islands close to the earthquake due to the tsunami. A volcanic eruption took place at roughly the same time and 'the eruption was followed by a tidal wave, which did infinitely greater damage to the plantations than the eruption' (SYDNEY MORNING HERALD (1901b). The tsunami was observed as both coastal run-up and on tide gauge records in Hawaii (Table 9).

COUNTRY	LOCATION	MAX WATER HEIGHT (M)	TYPE
Solomon Islands	Santa Cruz Islands	Obs	Run-up
Vanuatu	Vanuatu Islands	Obs	Run-up
USA	Honolulu, Hawaii	0.12	Gauge
USA	Honuapo, Hawaii	Obs	-
USA	Hookena, Hawaii	Obs	-
USA	Hoopuloa, Hawaii	1.20	Run-up
USA	Kailua-Kona, Hawaii	1.20	Gauge
USA	Keauhou, Hawaii	Obs	-
USA	Mahukona, Hawaii	Obs	-
USA	Napoopoo, Hawaii	Obs	-

Table 9: Observations of the 9 August 1901 tsunami (adapted from NGDC tsunami database). There is no record of this event in the New Zealand historical tsunami database (DOWNES, PERS COMM.).

The observed tsunami amplitudes in Hawaii are significantly larger than those of the 2009 Mw 8.1 Samoa earthquake, and on this basis we favour the interpretation of a moment magnitude for this event around 8.4.

4.4 Magnitude frequency of seismicity data 1976-2009

The Global CMT catalog was searched for thrust events (T-axis plunge between 45 and 90 degrees) on the southern New Hebrides from 1976 to 2009 inclusive between 21-23.5 °S and 169-174 °E, and this search yielded 156 events. It was found that the selected earthquakes were largely concentrated in the west of the search region, between 169-171 °E. The 1901 earthquake occurred in this area of higher seismicity; at M8.4 it would have released approximately 5m of slip (representing a minimum of 106 years of slip accumulation at the convergence rate of 47 mm/yr in the unlikely situation of full interseismic coupling on the interface).

The total seismic moment release in the full set of selected events is $6.57*10^{27}$ dyn-cm. Assuming a down-dip width of 60km this is equivalent to an average annual slip of 18 mm on the subduction interface that is released in such events, or about 38% of the plate convergence rate (higher in the west, lower in the east). This does not tell us what proportion of the remaining slip is released aseismically, and what proportion is accumulated as strain to be released in larger events occurring on longer timeframes.

A plot of the cumulative number of events greater than or equal to a given magnitude over this 34-year period is shown in Figure 14. Below Mw 5.5 the catalog shows signs of incompleteness, and above Mw 6.5 there are insufficient events to produce reliable statistics. The trendline shown, based on all available datapoints implies a b-value of 0.73.

Figure 14

As we discussed in Section 3.4, we consider the extrapolation of magnitude frequency curves to significantly larger events to be of very limited reliability, especially where there is a change in earthquake scaling characteristics as happens here once we enter the domain where the typical earthquake width reaches the full down-dip extent of the coupled subduction interface. However, if we extrapolate the trendline to estimate the frequency of events greater than or equal to Mw 8.0 we find that such events are

expected approximately once every 28 years, at odds with the observation of only one such event in the past century (Section 4.3).

4.5 Tsunami scenario results

In order to create scenario events for tsunami modelling we have divided the southern New Hebrides into three segments D,E and F, each about 200km long. Since this subduction zone does not undergo sharp changes in strike and has a relatively uniform cross-section, this division into segments is mostly for the purposes of illustration, and to test the sensitivity of the tsunami modelling results to rupture of different portions of the trench. We note that the westernmost segment (D) is the site of the largest historical earthquake on this subduction zone in 1901, and that the present-day level of seismicity is noticeably greater within this segment than those to the east. We again consider a more severe scenario involving the rupure of all three segments (D+E+F). A rupture that extends into (or emerges from) the main New Hebrides Trench (ie north of 22ºS) also cannot be ruled out. It is important to note that the convergence rate on the New Hebrides Trench west of 170°E is much greater than on the southern New Hebrides Trench, due to rapid clockwise rotation of Vanuatu (e.g., CALMANT ET AL., 2003; Figure 12).

Scenario earthquakes have been constructed for the southern New Hebrides subduction zone with the rupture properties summarized in Table 10 and illustrated in Figure 13.

Table 10 Scenario earthquakes along southern New Hebrides subduction zone

Scenario	Segment	Unit Patch	Length	Width	slip	Magnitude
5	D	NH06, NH07	200 km	60 km	3.5 m	Mw 8.15
6	E	NH04, NH05	200 km	60 km	3.5 m	Mw 8.15
7	F	NH02, NH03	200 km	60 km	3.5 m	Mw 8.15
8	D+E+F	NH02-NH07	600 km	60 km	10.7 m	Mw 8.8

Scenario 5 is an Mw 8.15 earthquake occurring at the western part of the southern New Hebrides subduction zone (Segment D). The rupture area covers a 200km-by-60km portion of the southern New Hebrides plate interface which corresponds to unit patches of NH06 and NH07. Earthquake scenario 6 occurs near the middle of the southern New Hebrides interface with magnitude Mw 8.15. The rupture area comprises unit patches NH04 and NH05 with an area of 200 km long and 60 km wide (Segment E). Earthquake scenario 7 with magnitude Mw 8.15 ruptures the eastern portion of the southern New Hebrides subduction interface (Segment F), covering an 200km-by-60km area which comprises unit patches NH02 and NH03. A more severe scenario, earthquake scenario 9, is assumed to rupture the entire southern New Hebrides Trench (Segment D+E+F) with magnitude Mw 8.8.

For each scenario earthquake, wave evolution over a 10-hour duration has been modeled in order to estimate the maximum wave amplitude on and offshore, and hence evaluate the tsunami hazard to New Zealand (Figures 15-18).

Figure 15

For scenario earthquake 5 (Segment D; Figure 15), numerical simulation shows that the majority of tsunami energy travels to the southwest and northeast due to the trench orientation, and New Zealand is not in its path. Only a small fraction of energy is directed to the coast of Northland under the wave-guiding influence of the Norfolk Ridge and the Three Kings Ridge. In the coastal areas of Northland, water levels will be elevated by 1.0-2.0 meters. In other parts of North Island, water level increment is well below 1.0 meter.

Figure 16

In Scenario 6, the earthquake ruptures the middle section of the southern New Hebrides plate interface (Segment E; Figure 16). Compared with Scenario 5, more tsunami energy is directed towards the Northland region of New Zealand due to the trench orientation, together with the wave-guiding effect of the Norfolk Ridge and the Three Kings Ridge. Tsunami runup heights of about 2.0-3.0 meters on the north and

west coasts of the Aupouri Peninsula are significantly larger than those along the northeastern coast of Northland and the other coastal areas of North Island, which are around 1.0 meters or below.

Figure 17

In Scenario 7, the earthquake ruptures the eastern section of southern New Hebrides plate interface (Segment F; Figure 17). Numerical simulation shows that the tsunami travels directly towards the North Island of New Zealand. The distribution pattern of the maximum water level along the coasts is similar to that of Scenario 6 (Segment E). The amplitude however is much larger. Due to the wave guiding effect of the Norfolk Ridge and the Three Kings Ridge, more energy is directed towards the Northland region. Tsunami runup heights around 5.0 meters are observed along the west coast of the Aupouri Peninsula. Along the northeastern coast of Northland, tsunami amplitudes are significantly lower, around 1.0 meters above the normal level.

Figure 18

In the worst scenario, the entire southern New Hebrides subduction interface ruptures, which corresponds to an Mw 8.8 earthquake (Segment D+E+F; Figure 18). Due to the wave-guiding effect of the Norfolk Ridge and the Three Kings Ridge, more energy is directed towards the Northland region. Tsunami runup heights of about 10.0-15.0 meters are observed along the coast of the northwestern tip of Northland and of about 3.0-5.0 meters at other parts of the southwestern coast of Northland. Along the northeastern coast, tsunami runup heights are significantly lower. Along most of the coastline, the runup height is around 3.0-5.0 meters above the normal level, although at some places it is up to 7.0 meters.

5. Discussion

The scenario models demonstrate that there is a clear potential risk to New Zealand from both the Kermadec Trench and the Southern New Hebrides Trench. The risk from the Southern New Hebrides is mostly confined to sparsely populated Aupouri

Peninsula of northern Northland, while the Kermadec Trench poses a risk to most of northern New Zealand, especially to the Coromandel, Great Barrier Island, and Northland regions.

Travel times between the Kermadec Trench and these high-risk locations are in the 45 min to 2 hour range, which permits some form of warning to be issued, though current technology will mean that there will be a great deal of uncertainty about the source during this timeframe. The best prospect for quantifying tsunami generation in the minutes following an earthquake is via DART buoys. One NOAA DART buoy is currently stationed close to the middle of the Kermadec Trench at 33.005 S 172.985 W (DART 54401; Figure 6), and a second is placed close to the Tonga Trench at 22.993 S 168.098 W (DART 51426). Our results show that northern New Zealand is more susceptible to waves arising from slip on the southern part of the Kermadec Trench than to slip on portions of the trench further north, and better information on tsunami generated by earthquakes in that area could be obtained by locating a DART buoy in the vicinity of segment A.

The single Raoul GPS site provides the only geodetic measurement of inter-plate coupling along the Kermadec Arc, and this site velocity is consistent with strong interseismic coupling on the central portion of the Kermadec Trench. Raoul is an active volcano which could cause some transient (volcanic) deformation to influence the site velocity there; however, the movement of this GPS site appears to have followed a reasonably steady long-term trend from 1996 to the present, and does not appear to be strongly influenced by volcanic activity. Alternative GPS sites on the Kermadec Arc are severely limited due to difficulty of access, yet the question of whether the apparent coupling at Raoul is typical of the arc as a whole, or a local exception, is critical for the assessment of tsunami hazard posed by the Kermadec Arc. Seabed geodetic measurements have been used to infer interseismic coupling on the subduction margin offshore Chile (GAGNON ET AL., 2005), and could provide an answer to this key question, but ocean floor geodesy is very expensive.

Our understanding of the subduction zone can also be improved through a better theoretical understanding of the processes which control subduction interface

earthquakes and the accumulation of strain at the plate interface. However great care must be taken in the application of these theories, since for most subduction zones there is insufficient historical data to verify them (McCaffrey, 2007).

With regard to the Kermadec Trench we find that the most widely held view, that this trench has relatively low seismic coupling and does not produce earthquakes with magnitudes greater than about Mw 8½ (eg Berryman, 2005), is compatible with the available magnitude-frequency data, but that an alternative picture with stronger average seismic coupling and greater maximum earthquake magnitudes is also consistent (Appendix I). At the present time we favour the traditional viewpoint, but this would be reversed if it was found that strong interseismic coupling, such as found at Raoul, was typical along the trench.

A number of paleotsunami sites have been found in those parts of New Zealand that we have found to be among the most vulnerable to Kermadec Trench tsunami, ie the Coromandel Peninsula, Great Barrier Island, and Northland (Goff, 2008; Goff et al., 2010). The most notable of these is at Hendersons Bay in Northland where a tsunami deposit is located at 32m above sea level. Several of these sites suggest tsunami run-ups in excess of 10m. Most of these sites have estimated event ages in the range (AD 1400 – 1500; Goff 2008). Our modelling suggests that a Kermadec Trench earthquake would need to be in excess of Mw 9 to explain these deposits. Indeed, the distribution of maximum water levels in our Scenario 4 shows a striking similarity to the distribution of paleotsunami run-up heights in ~1450 AD as shown in Figure 7 of Goff et al. (2010). However before drawing any conclusions it is necessary to examine the question of whether there are other plausible sources for these deposits. Thus far attempts to explain them as caused by landslides or volcanic events are inconclusive. Landslide tsunami sources tend to concentrate high run-ups within a small range of coastline (Okal and Synolakis, 2004), and volcanic sources tend to radiate tsunami energy in a fashion which causes the run-up height to attenuate rapidly with distance.

Walters et al. (2006) modelled the tsunami propagation from a Mw 8.5 subduction zone earthquake on the southern part of the Kermadec Trench into the Bay of Plenty.

In their model the vertical uplift caused by the earthquake appears to be in excess of 7m, and the subsequent maximum water level at the Bay of Plenty coastline was found to be around 5m. This is in contrast to our results which suggest maximum water elevations of 1-2m in the Bay of Plenty following an earthquake of this magnitude; the results of WALTERS ET AL. (2006) are much more consistent with the results of our Mw 9.4 scenario.

For detailed Probabilistic Tsunami Hazard Analysis (PTHA) in regions where there is substantial epistemic uncertainty in the source parameters a logic-tree approach is preferred (BERRYMAN, 2005; GEIST AND PARSONS, 2006; ANNAKA ET AL, 2007). Weights are associated to discrete branches of the tree representing the alternative hypotheses for parameters that determine the tsunami source statistics. We have developed a relatively simple logic tree for each of the Kermadec Arc and Southern New Hebrides source regions (Appendix I), for use in future probabilistic studies into tsunami hazard in northern New Zealand. It is important to note that each complete branch through the logic tree represents not a single scenario, but a particular statistical model of the source region including aleatory variability due to the random nature of earthquakes. Each individual statistical model may then be approximated using a large number of different scenarios in eg a Monte Carlo analysis. It should also be understood that the logic tree is a reflection of the opinions of its creators, and is not something which can be scientifically derived from first principles, though in the Appendix we do our best to explain the reasoning behind our choices.

6. Conclusions

The Kermadec and southern New Hebrides subduction margins are oriented in such a way that a sufficiently large earthquake would threaten the northern regions of New Zealand with destructive tsunami waves. In the historical record, complete only over the last 150 years or so, only the 1976 Kermadec earthquake was sufficient to cause minor tsunami damage, though our modelling suggests that the same size of earthquake would cause significantly more tsunami damage if it occurred further south on the Kermadec Trench. However, the historical record is short compared to the return time for major subduction zone earthquakes, and therefore too short to be

used in isolation to draw conclusions about the potential for future tsunami. To provide additional information we have derived estimates of convergence rates and interseismic fault coupling on the subduction interface from block modelling of earthquake slip vector data, transform fault orientations, and GPS velocities. This clearly demonstrates that there is strong interseismic coupling on the subduction interface beneath the Kermadec Islands. If this interseismic coupling occurs over long portions of the margin (and isn't just isolated to the Raoul Island region) elastic strain energy accumulating over long time frames could lead to large magnitude (Mw >8.5) events. This is not inconsistent with the fact that such large events have not been observed in the past 150 years (see Appendix). However caution is needed since the key GPS site for this work is on an active volcano (subject to other forms of deformation), and located in the area that has seen the largest historical earthquakes and may therefore be atypical of the trench as a whole. The comparison of run-up heights in our largest scenario event with the paleotsunami run-up data assigned to a tsunami in approximately 1450AD (GOFF ET AL., 2010) shows an intriguing similarity in distribution and scale. In light of the possible hazard implications we recommend that research be focussed on testing whether other possible sources could have created a similar distribution, and searching for other signatures of a large subduction zone earthquake in the 15th century such as co-seismic uplift on the Kermadec Islands or the East Cape of New Zealand. Less evidence is available to constrain the future size of earthquakes on the southern New Hebrides, though we demonstrate that the focussing effect of the undersea Three Kings Ridge leads to focussing of the largest tsunami waves on the sparsely populated coasts of the far north of New Zealand.

Acknowledgements

This work was funded by the New Zealand Earthquake Commission, and the New Zealand Foundation for Research, Science and Technology. We thank Mike Rosenberg, Colin Wilson, Stewart Bennie, and Todd Chandler for collecting the GPS data at Raoul Island. We thank Kate Clark and John Beavan for helpful reviews of the manuscript.

Appendix I: Logic trees for Kermadec Trench and southern New Hebrides earthquake sources

In order to quantitatively analyse the tsunami hazard to New Zealand from the Kermadec Trench and the southern New Hebrides, logic trees have been developed for the relevant earthquake source parameters. The logic trees represent the collective opinions of the scientists involved, after studying the available seismic and geodetic data.

A truncated Guttenberg-Richter distribution was chosen as the most suitable form for the statistical distribution of large earthquakes (Mw >8) in these source regions, and a b-value of 1 was assumed, matching the global magnitude-frequency distribution.

The plate convergence rates for both sources are accurately known, making it possible to specify the source magnitude-frequency distributions using just the maximum-magnitude and the seismic coupling coefficient for each source.

Figure A1

For each source a range of maximum magnitudes was considered, up to the point where scaling rules suggest a single rupture would span the entire source region, and extending no lower than the largest historical events. A range of coupling coefficients, representing weak (0.3), moderate (0.6), and strong coupling (0.9) were selected. Weights were then assigned to each combination of maximum magnitude and coupling coefficient (Figures A1 and A2).

Figure A2

For the Kermadec Trench the rate at which each combination of maximum magnitude and coupling coefficient produces earthquakes of magnitude greater than 8 was plotted (Figure A3). Historical data was judged to favour logic-tree branches that

produced average intervals for Mw >8 in the 50-100 year range, and these branches were assigned the majority of weighting.

Figure A3

Within the set of logic-tree branches that are consistent with the historical data we find branches with source parameters corresponding to the conventional interpretation that the Kermadec Trench has a relatively low maximum magnitude (< 8.5-8.6; eg BERRYMAN, 2005) and weak coupling, but we also find branches corresponding to an alternative interpretation where the Trench has a high maximum magnitude. In this latter view the reason that few earthquakes greater than Mw 8 have been historically observed is a consequence of the short observation time. In the logic-tree most weight was assigned to the established viewpoint, but some was also given to this alternative picture. It was felt that should the maximum magnitude be large then the seismic coupling would probably have to be relatively strong, as weak coupling would most likely represent small strongly-coupled asperities surrounded by large uncoupled regions, and this would be unlikely to allow large ruptures to develop. The weights for these branches were selected correspondingly. This picture of relatively strong coupling matches the observations from Raoul, and much more weight would be assigned to the high maximum magnitude and strong coupling combination if it was found that strong coupling exists at other trench locations.

For the southern New Hebrides, the combination of a short historical and instrumental record and a relatively short section of subduction zone, provides insufficient evidence with which to preferentially weight the maximum magnitude branches to the logic tree; in this situation we have selected a uniform distribution of weights between the largest historical event and the magnitude of a rupture spanning the full subduction zone. For the coupling coefficients we have placed greater weights on the low and medium strength coupling options in response to the elastic block modelling (Figure A2).

References

ABE, K. (1975). Reliable estimation of the seismic moment of large earthquakes. J. Phys. Earth, 23, 381-390.

ALTAMIMI, Z., SILLARD, P. AND BOUCHER C., ITRF2000: A new release of the International Terrestrial Reference Frame for earth science applications, J. Geophys. Res., 107(130), 2214, doi:10.1029/2001J1200561, 2002.

ANNAKA, T., SATAKE, K., SAKAKIYAMA, T., YANAGISAWA, K., SHUTO, N. (2007) Logic-Tree approach for probabilistic tsunami hazard analysis and its applications to the Japanese coasts. *Pure Appl Geophys* 164, 577–592

AUZENDE J.M., PELLETIER, B. LAFOY, Y. (1994) Twin active spreading ridges in the North Fiji Basin, Geology 22, 63-66.

BEAVAN, J., TREGONING, P., BEVIS, M., KATO, T., MEERTENS, C. (2002), Motion and rigidity of the Pacific Plate and implications for plate boundary deformation, *Journal of Geophysical Research, 107*(130), 2261, doi: 10.1029/2001J1200282

BEVIS, M., TAYLOR, F.W., SCHUTZ, B.E., RECY, J. , ISACKS, B.L., HELU, S., SINGH, R., KENDRICK, E., STOWELL, J., TAYLOR, B., AND CALMANT, S. (1995), Geodetic observations of very rapid convergence and back-arc extension at the Tonga arc: *Nature, v. 374,* p. 249-251.

BERRYMAN, K. (Compiler), 2005. "Review of Tsunami Hazard and Risk in New Zealand". Institute of Geological & Nuclear Sciences, Client Report 2005/104, Wellington

BIRD, P. (2003), An updated digital model of plate boundaries, *Geochem. Geophys. Geosyst., 4(3)*, doi:10.1029/2001GC000252.

BONNARDOT, M.-A, REGNIER, M., RUELLAN, E., CHRISTOVA, C. AND TRIC, E. (2007), Seismicity and state of stress within the overriding plate of the Tonga-Kermadec subduction zone, *Tectonics,* doi:10.1029/2006TC002044

BOSSU, R. (2000), A simple approach to contrain the position and the geometry of the seisogenic structures: application to the Karthan volcano (Grande Comores Island, Mozambiguqe Channel), *J. Seismol.*, 4, 41-48.

CALMANT, S., PELLETIER, B., LEBELLEGARD, P., BEVIS, M., TAYLOR, F.W., PHILLIPS, D.A. (2003), New insights on the tectonics along the New Hebrides subduction zone based on GPS results: *J. Geophys. Res., v. 108(18),* doi:10.1029/2001J1200644.

CHO, Y.-S. (1995). *Numerical simulations of tsunami and runup*. PhD thesis, Cornell University.

DE RONDE, C. E. J., BAKER, E. T., MASSOTH, G. J., LUPTON, J. E., WRIGHT, I. C., SPARKS, R. J., BANNISTER, S. C., REYNERS, M. E., WALKER, S. L., GREENE, R. R., ISHIBASHI, J. FAURE, K., RESING, J. A. AND LEBON, G. T. (2007). Submarine hydrothermal activity along the mid-Kermadec Arc, New Zealand: large-scale effects on venting. *Geochem. Geophys. Geosyst*. 8, Q07007, doi: 10.1029/2006GC001495.

DELTEIL, J., RUELLAN, E., WRIGHT, I., AND MATSUMOTO, T. (2002), Structure and structural development of the Havre Trough (SW Pacific), *J. Geophys. Res., 107(B8),* doi: 10.1029/2001J1200494.

DUDA, S.J. (1965), Secular seismic energy release in the circum-Pacific belt. Tectonophysics, vol. 2, no. 5, p. 409-452.

DZIEWONSKI, A.M., AND WOODHOUSE, J.H (1983), Studies of the seismic source using normal-mode theory, *in:* Kanamori, H., and Boscie, E., eds. *Earthquakes: Observation, Theory, and Interpretation: Notes from the International School of*

Physics 'Enrico Fermi' (1982: Varenna, Italy), pp. 45-137, North Holland Publishing Co., Amsterdam.

ENGDAHL, E., VAN DER HILST, R., AND BULAND, R. (1998), Global teleseismic earthquake relocation with improved travel times and procedures for depth determination, *Bull. Seismol. Soc. Am.*, 88, 722-743.

FEIGL, K., AGNEW, D., BOCK, Y., DONG, D., DONNELLAN, A., HAGER, B., ET AL. (1993). Space geodetic measurement of crustal deformation in central and southern California, 1984–1992. *J. geophys. Res , 98* (132), 1677-712.

GAGNON, K., CHADWELL, C.D., AND NORABUENA, E. (2005), Measuring the onset of locking in the Peru-Chile Trench with GPS and acoustic instruments, *Nature, 434,* 205-208.

GEIST, E.L., AND PARSONS, T. (2006). Probabilistic analysis of tsunami hazards. *Natural Hazards* 37, 277–314.

GOFF, J.R. (2008). The New Zealand Palaeotsunami Database. *NIWA Technical Report 131.* 24p, database.

GOFF, J., PEARCE, S., NICHOL, S.L., CHAGUÉ-GOFF, C., HORROCKS, M. AND STROTZ, L. (2010), Multi-proxy records of regionally-sources tsunamis, New Zealand. *Geomorphology*, 118, 369-382.

GUTENBERG, B. (1956), Great Earthquakes, 1896-1903; Transactions of the American Geophysical Society, Vol 37, p603-614.

HANKS, T.C. AND BAKUN, W.H. (2002), A bilinear source-scaling model for M-log A observations of continental earthquakes, Bull. Seismol. Soc. Am. 92(5), 1841–1846, illus. incl. 1 table, 28 refs.

HECK, N. (1947), List of seismic sea waves, *Bull. Seism. Soc. Amer.* 37, 269-286.

HERRING, T.A., DAVIS, J.L., SHAPIRO, I.I. (1990), Geodesy by radio interferometry: The application of Kalman filtering to the analysis of very long baseline interferometry data, *Journal of Geophysical Research, 95*, 12561-12581.

HERRING, T.A., (2001), GLOBK global Kalman filter VLBI and GPS analysis program, version 5.03, Massachusetts Institute of Technology, Cambridge.

KUMIZI, I., COX, D.C. AND PARARAS-CARAYANNIS, G. (1967) Preliminary Catalog of Tsunamis Occurring in the Pacific Ocean, HIG-67-10, Hawaii Institute of Geophysics, University of Hawaii, Honolulu, Hawaii, 275 p. Bibliography to the Preliminary Catalog of Tsunamis Occurring in the Pacific Ocean, December 1967, 27 p.

KENNETT, B.L.N. AND CUMMINS, P.R. (2005), The relationship of the seismic source and subduction zone structure for the 2004 December 26 Sumatra-Andaman earthquake, Earth and Planetary Science Letters, Volume 239, Issues 1-2, 30, Pages 1-8,

KING, R.W., AND BOCK, Y. (2002), Documentation for the GAMIT GPS analysis software, release 10.04, Massachusetts Institute of Technology, Cambridge, Massachusetts.

LANDER, J. F., AND LOCKRIDGE, P.A. (1989), United States Tsunamis (Including United States Possessions) 1690-1988, National Oceanic and Atmospheric Administration, National Geophysical Data Center, Boulder, Colorado, USA, Publication 41-2, 265 p.

LAWVER, L.A., HAWKINS, J.W. AND SCLATER, J. G. (1976), Magnetic anomalies and crustal dilation in the Lau Basin, *Earth Planet. Sci. Lett., 33*, 27-35.

LIU, P.L.-F., CHO, Y. -S. AND FUJIMA, K. (1994). Numerical solutions of three-dimensional run-up on a circular island, *Proceedings of International Symposium*: *Waves-Physical and Numerical Modellin*g, pp. 1031-1040, Canada.

LIU, P. L.-F., CHO, Y.-S., YOON, S. B. AND SEO, S. N. (1994). Numerical simulations of the 1960 chilean tsunami propagation and inundation at hilo, hawaii. In *Recent Development in Tsunami Research*, pages 99–115. Kluwer Academic Publishers, 1994.

LIU, P. L.-F., CHO, Y-S., BRIGGS, M.J., SYNOLAKIS, C.E., AND KANOGLU, U. (1995), "Run-up of Solitary Waves on a Circular Island", *J. Fluid Mechanics*, 302, 259-285.

LOMNITZ, C. (1974), Development in Geotectonics #5, Global Tectonics and Earthquake Risk, Elsevier Scientific Publishing Co., Amsterdam, The Netherlands.

LUNDGREN, P. R., OKAL, E. A., AND WIENS, D. A. (1989), *Rupture Characteristics of the 1982 Tonga and 1986 Kermadec Earthquakes,* J. Geophys. Res. *94,* 15521-15539.

MCCAFFREY, R. (2002), Crustal block rotations and plate coupling: *in* Stein, S., and Freymueller, J., eds., Plate Boundary Zones, AGU Geodynamics Series v. 30, p. 100-122.

MCCAFFREY, R. (2007), The Next Great Earthquake, *Science* 23 March 2007 315: 1675-1676

MCCLUSKY, S., and 27 others (2000), Global Positioning System constraints on plate kinematics and dynamics in the eastern Mediterranean and Caucasus, *Journal of Geophysical Research, 105*, 5695-5719.

NATIONAL EARTHQUAKE INFORMATION CENTER (NEIC) 1971 to present Preliminary Determination of Epicenters (PDE), a weekly and monthly publication, National Earthquake Information Center, U.S. Geological Survey, Golden, Colorado.

NICHOLSON, T., (2006). Application of 3D empirical travel times to routine event location. *Physics of the Earth and Planetary Interiors*, 158, 67-74.

OKADA, Y., (1985). Surface deformation due to shear and tensile faults in a half-space, *Bull. Seismol. Soc. Am.*, *75*, 1135-1154.

OKAL, E.A., BORRERO, J.C., SYNOLAKIS, C.E.(2006) Evaluation of Tsunami Risk from Regional Earthquakes at Pisco, Peru, *Bulletin of the Seismological Society of America* 96: 1634-1648

OKAL, E.A., AND SYNOLAKIS, C.E., (2004), Source discriminants for nearfield tsunamis, Geophysical Journal International, 158, 899–912.

PARSON, L. M. AND HAWKINS, J.W. (1994), Two-stage ridge propagation and the geological history of the Lau back-arc basin, *Proc. Ocean Drill. Program Sci. Results, 135*, 819–828.

PELLETIER, B. AND LOUAT, R. (1989), Seismotectonics and present-day relative plate motions in the Tonga-Lau and Kermadec-Havre region, *Tectonophysics, 165*, 237-250.

PELLETIER, B., CALMANT, S. AND PILLET, R. (1998), Current tectonics of the Tonga-New Hebrides region: *Earth and Planetary Sci. Letters, 164*, p. 263-276.

POWER, W., DOWNES, G. AND STIRLING, M., (2007) Estimation of Tsunami Hazard in New Zealand due to South American Earthquakes, Pure appl. geophys. 164 p 547–564

PRESS, W.H., FLANNERY, B.P., TEUKOLSKY, S.A., AND VETTERLING, W.T. (1989), Numerical Recipes: Cambridge University Press, Cambridge.

RICHTER, C.F. (1958), Elementary Seismology, W.H. Freeman and Company, San Fransisco, CA.

ROMANOWICZ, B. (1992), Strike-slip earthquakes on quasi-vertical transcurrent faults: Inferences for general scaling relations, Geophys. Res. Lett. 19, 481–484.

ROMANOWICZ, B. (1994), Comment on 'A reappraisal of large earthquake scaling' by C. Scholz, Bull. Seismol. Soc. Am. 84, 1675–1676.

SCHERWATH, M., KOPP, H., FLUEH, E. R., HENRYS, S. A. AND SUTHERLAND, R. (2008), Structure and Deformation of the Hikurangi-Kermadec Subduction Zone - Transitions Revealed by Seismic Wide-angle Data. *Eos Trans. AGU, 2008 Fall Meeting. Suppl.*, Abstract T23A-1997.

SCHOLZ, C.H. (1982), Scaling laws for large earthquakes; consequences for physical models, Bull. Seismol. Soc. Am. 72(1), 1–14

SCHWARTZ, D. AND COPPERSMITH, K. (1984), Fault Behavior and Characteristic Earthquakes: Examples From the Wasatch and San Andreas Fault Zones, J. Geophys. Res., 89(19), 5681-5698.

SHOR, G.G., KIRK, H.K., AND MENARD, H. W., (1971). Crustal structure of the Melanesian area. *J. Geophys. Res*., 76, 2562-2586.

SOLOVIEV, S.L., AND GO,CH.N. (1975) A catalogue of tsunamis on the eastern shore of the Pacific Ocean. Academy of Sciences of the USSR, Nauka Publishing House, Moscow, 204 p. [Canadian Translation of Fisheries and Aquatic Sciences No. 5078, 1984, translation available from Canada Institute for Scientific and Technical Information, National Research Council, Ottawa, Ontario, Canada K1A OS2, 293 p.]

SUBARYA, C, CHLIEH, M., PRAWIRODIRDJO, L., AVOUAC, J., BOCK, Y., SIEH, K., MELTZNER, A J., NATAWIDJAJA, D H. AND MCCAFFREY, R. (2006). "Plate-boundary

deformation associated with the great Sumatra–Andaman earthquake." *Nature*, 440, 46-51

THE SYDNEY MORNING HERALD, NEW SOUTH WALES, AUGUST 31, (1901a), An Island Cruise, A Tidal Wave. http://newspapers.nla.gov.au/ndp/del/article/14407034

THE SYDNEY MORNING HERALD, NEW SOUTH WALES, SEPTEMBER 4, (1901b), Volcanic Eruption at New Hebrides. http://newspapers.nla.gov.au/ndp/del/article/14407505

TAYLOR, F. W., BRIGGS, R. W., FROHLICH, C., BROWN, A., HORNBACH, M. J., PAPABATU, A. K., MELTZNER, A. J. AND BILLY, D. (2008), Rupture across arc segment and plate boundaries in the 1 April 2007 Solomons earthquake, *Nature Geoscience*, *1*, 253-257, doi:10.1038/ngeo159.

TITOV, V. V., MOFJELD, H. O., GONŹALEZ, F. I., AND NEWMAN, J. C. (1999), 'Offshore forecasting of Alaska-Aleutian Subduction Zone tsunamis in Hawaii'. NOAA Tech. Memo ERL PMEL-114, NOAA/Pacific Marine Environmental Laboratory, Seattle, WA.

TITOV, V. V., GONZALEZ, F. I., BERNARD, E. N., EBLE, M. C., MOFJELD, H. O., NEWMAN, J. C. AND VENTURATO, A. J. (2005), Real-Time Tsunami Forecasting: Challenges and Solutions. *Natural Hazards*, 35(1): 35-41.

TREGONING, P., LAMBECK, K., STOLTZ, A., MORGAN, P., MCCLUSKY, S.C., VAN DER BEEK, P., MCQUEEN, H., JACKSON, R.J., LITTLE, R.P., LAING, A., MURPHY, B. (1998), Estimation of current plate motions in Papua New Guinea from Global Positioning System observations, *Journal of Geophysical Research, 103*, 12181-12203.

WALTERS, R. A., GOFF, J. R., AND WANG, K. (2006), Tsunamigenic sources in the Bay of Plenty, New Zealand, Sci. Tsu. Haz., 24, 339–357.

WANG, X. AND LIU, P. L.-F. (2006). An analysis of 2004 sumatra earthquake fault plane mechanisms and indian ocean tsunami. *J. Hydraulic Res.*, 44(2):147–154, 2006.

WANG, X. AND LIU, P. L.-F. (2007), Numerical simulations of the 2004 indian ocean tsunamis - coastal effects. *Journal of Earthquake and Tsunami*, 1(3):273–297.

WANG, X.; ORFILA, A.; LIU, P.L.-F. (2008) Numerical simulations of tsunami runup onto a three-dimensional beach with shallow water equations. p. 249-253 IN: Liu, P.L.-F.; Yeh, H.H; Synolakis, C. (eds) *Advanced numerical models for simulating tsunami waves and runup*. Hackensack, NJ: World Scientific. Advances in coastal and ocean engineering 10.

WEISSEL, J. K. (1977), Evolution of the Lau Basin by the growth of small plates, *in Island Arcs, Deep Sea Trenches, and Back-Arc Basins, Maurice Ewing Ser., vol. 1*, edited by M. Talwani and W. C. Pitman III, pp. 429–436, AGU, Washington, D. C.

WIJETUNGE J.J., WANG X., LIU P.L.-F. (2008) Indian Ocean Tsunami on 26 December 2004: numerical modelling of inundation in three cities on the south coast of Sri Lanka. J Earthq Tsunami 2(2):133–155.

WRIGHT, I.C. (1993), Pre-spreading rifting and heterogeneous volcanism in the southern Havre Trough back-arc basin, *Mar. Geol., 113*, 179-200.

Figures

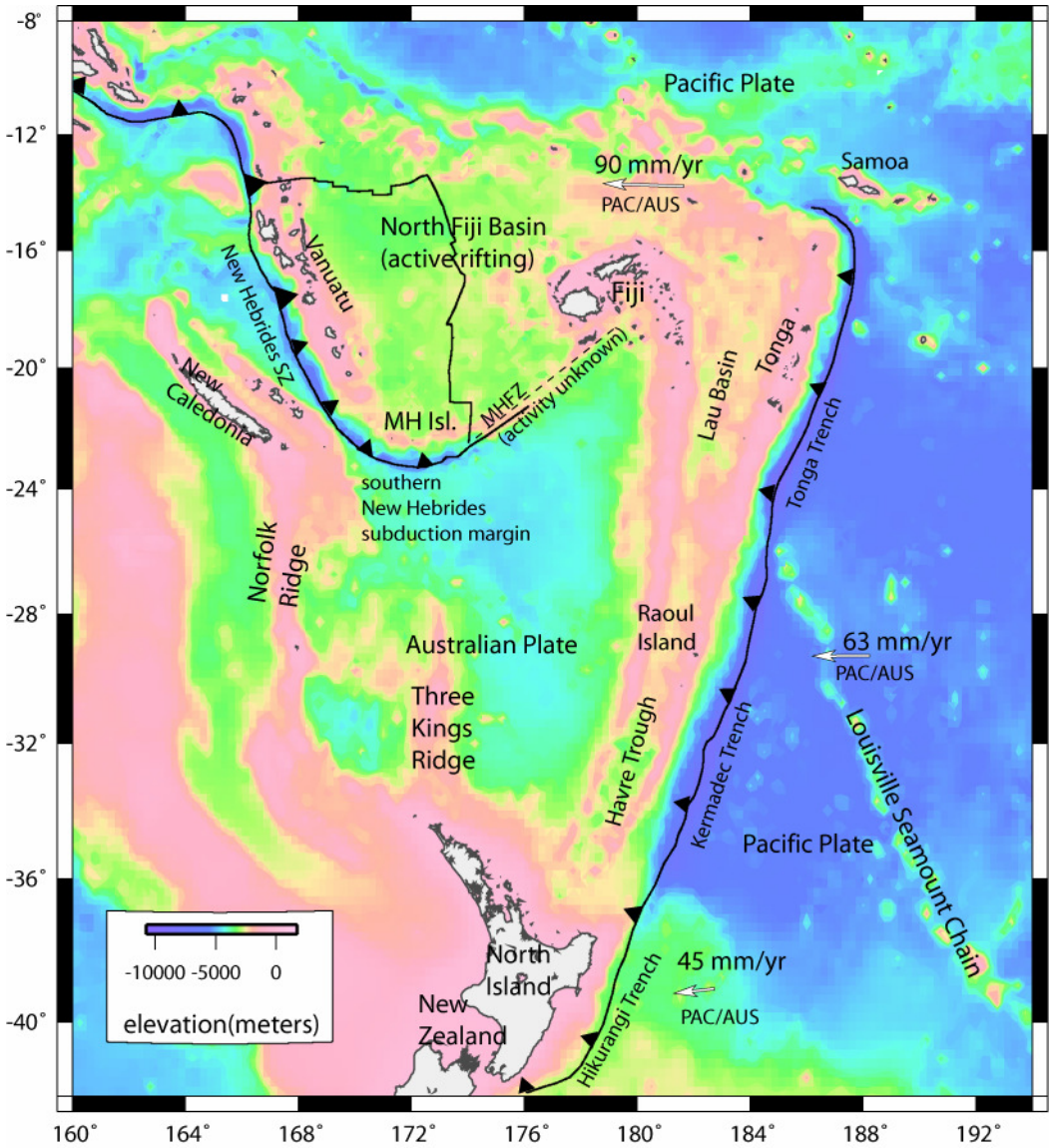

Figure 1 Tectonic setting of the Kermadec and New Hebrides plate margins. Black Triangles signify the over-riding plate at the regions' subduction margins. White arrows show predicted motion of the Pacific Plate relative to the Australian Plate. MH Isl. = Matthew Hunter Islands; MHFZ = Matthew Hunter Fracture zone; PAC = Pacific Plate; AUS = Australian Plate; SZ = subduction zone..

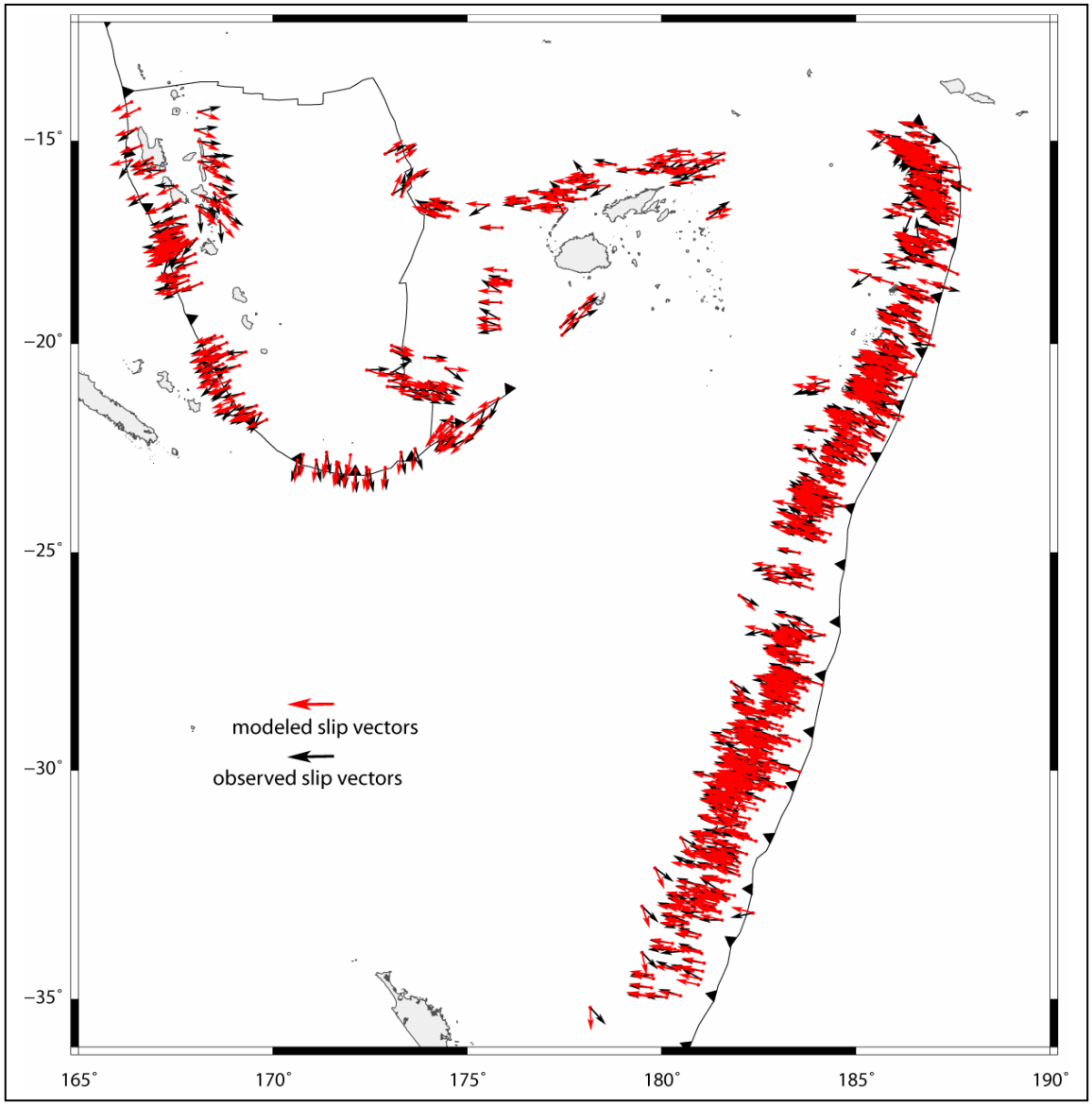

Figure 2: Earthquake slip vectors used in kinematic modelling (red = modelled; black = observed). Blue crosses show locations of major earthquakes described in text.

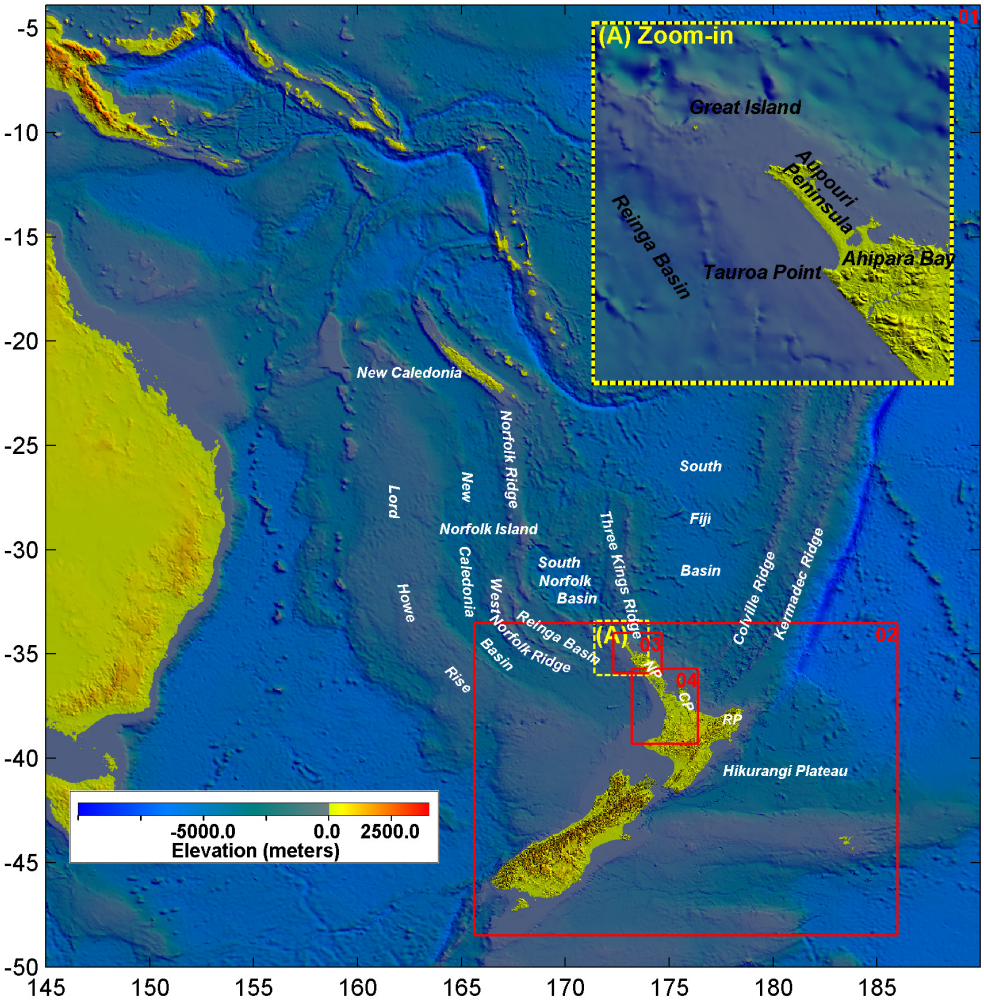

Figure 3: Nested grid configuration for tsunami modelling, with locations of bathymetric and topographic features referred to in the text. Red boxes represent nested grid regions with different spatial resolutions. The colour scale shows the water depth/land elevation in meters. CP = Coromandel Peninsula, NP = Northland Peninsula, RP = Raukumara Peninsula.

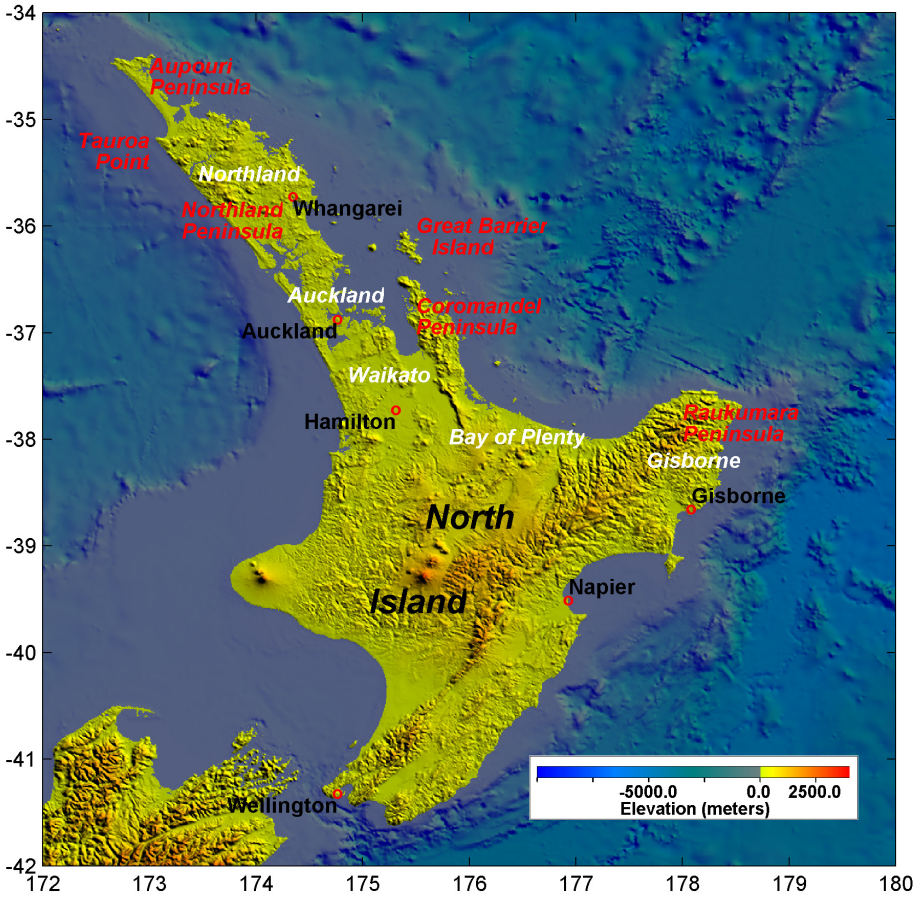

Figure 4: Locations in the North Island of New Zealand referred to in the text.

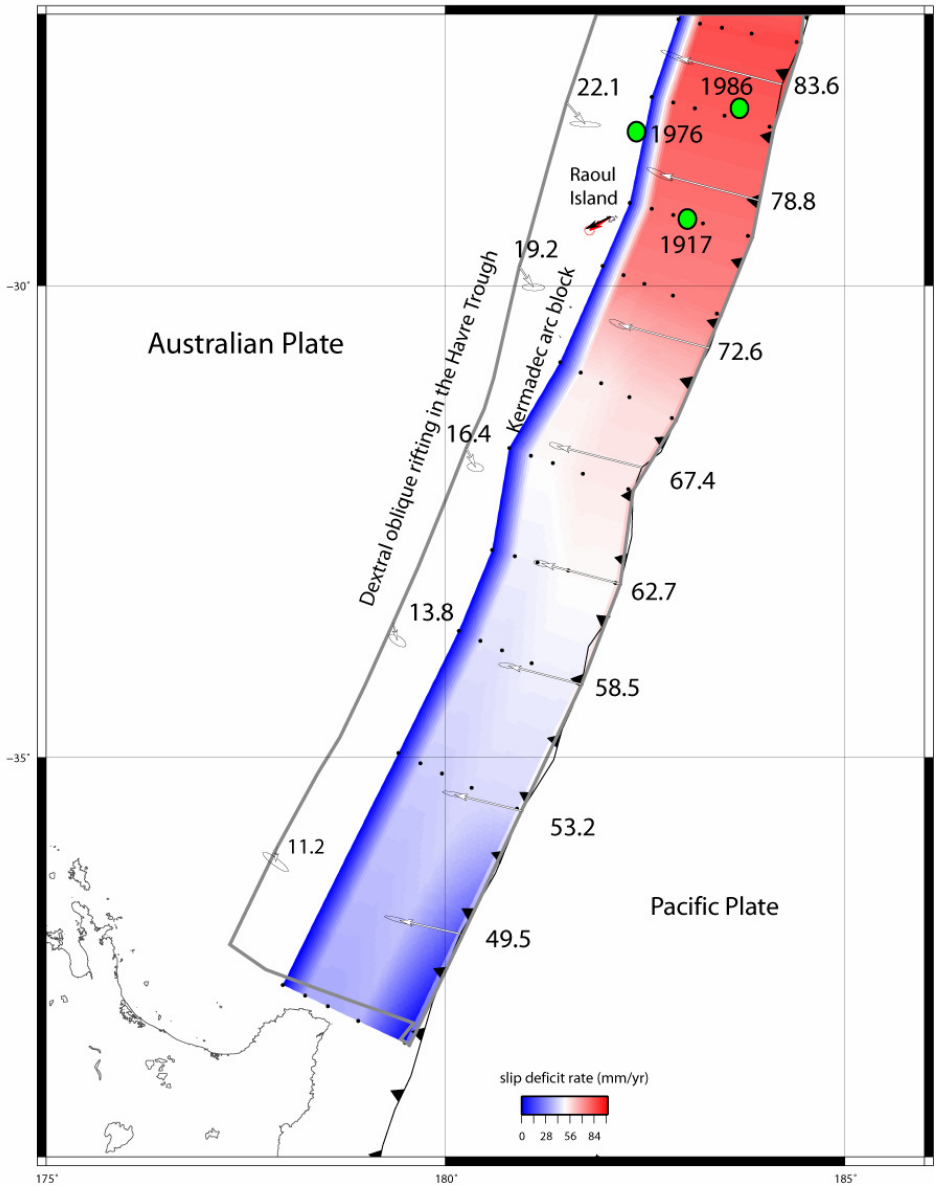

Figure 5: Plate kinematic and fault locking results from block modelling of earthquake slip vector data and GPS velocities. Black arrow at Raoul Island is the observed GPS velocity for that GPS site, while the red is the modelled velocity. White arrows on the boundaries are the long-term relative motion between adjacent blocks (labelled with rates in mm/yr). Green circles show the locations of historic earthquakes described in the text.

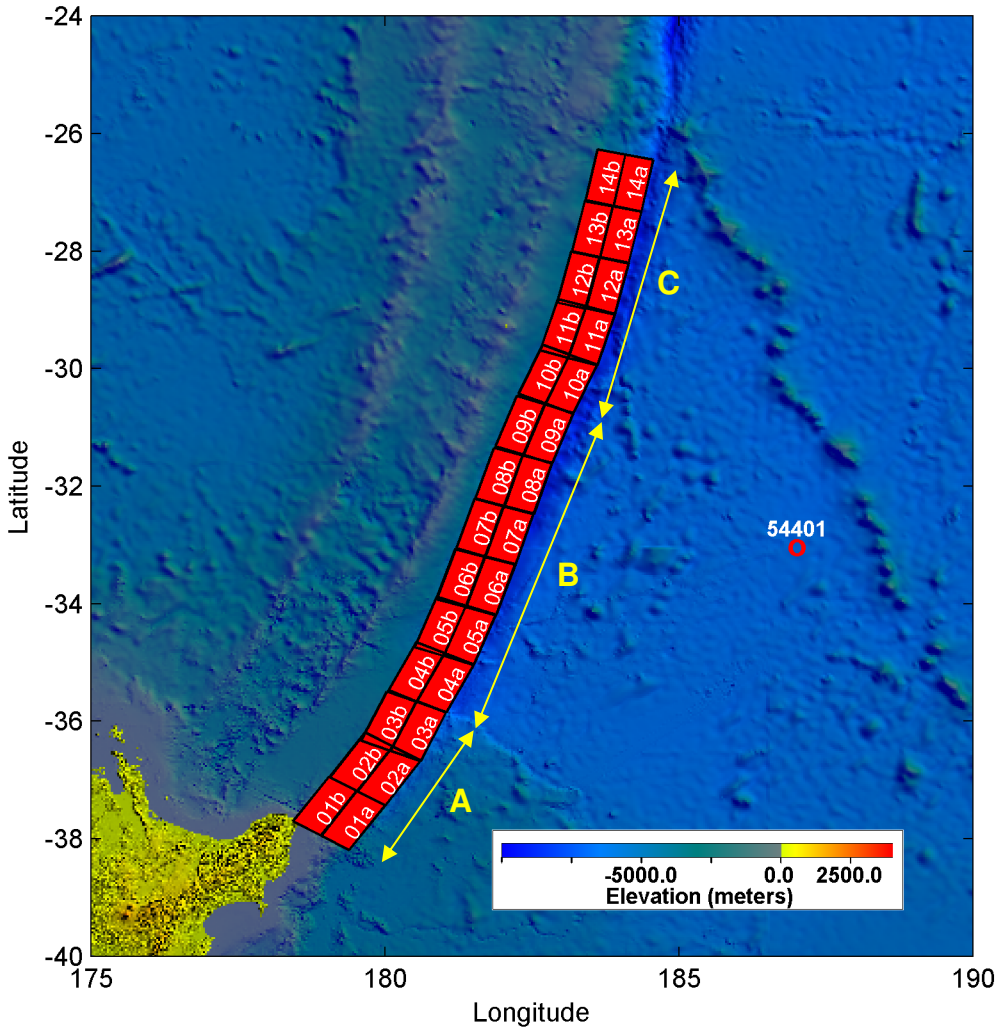

Figure 6: Illustration of 100km-by-50km unit patches along Kermadec subduction interface. The location of DART Buoy 54401 is also shown. A,B and C indicate the segmentation used for scenario events.

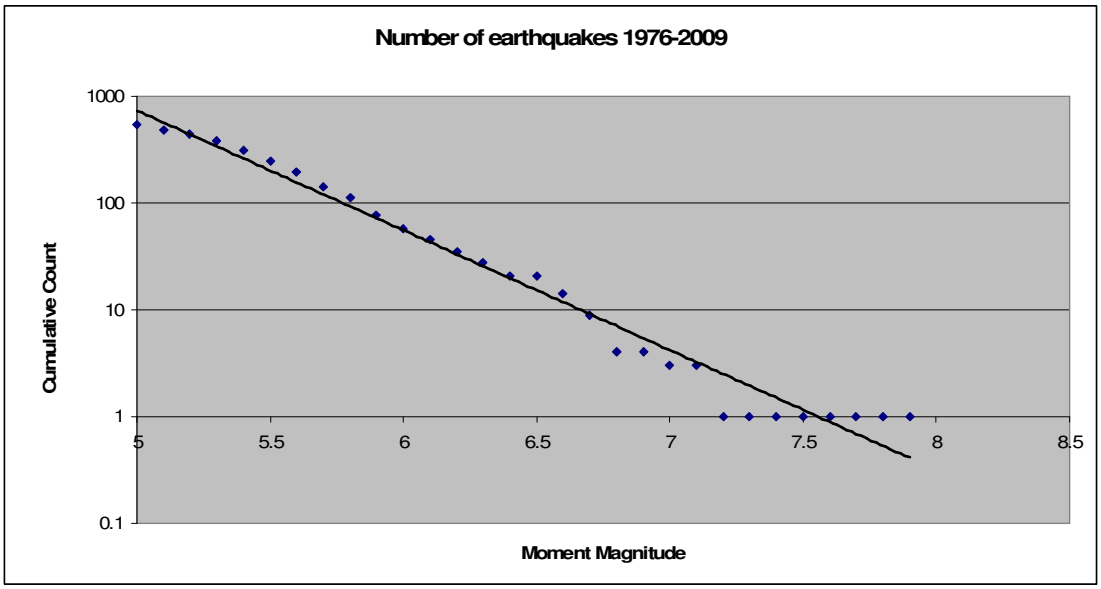

Figure 7. Cumulative number of subduction thrust earthquakes on the Kermadec Arc, for the period 1976-2009 inclusive, exceeding a given moment magnitude.

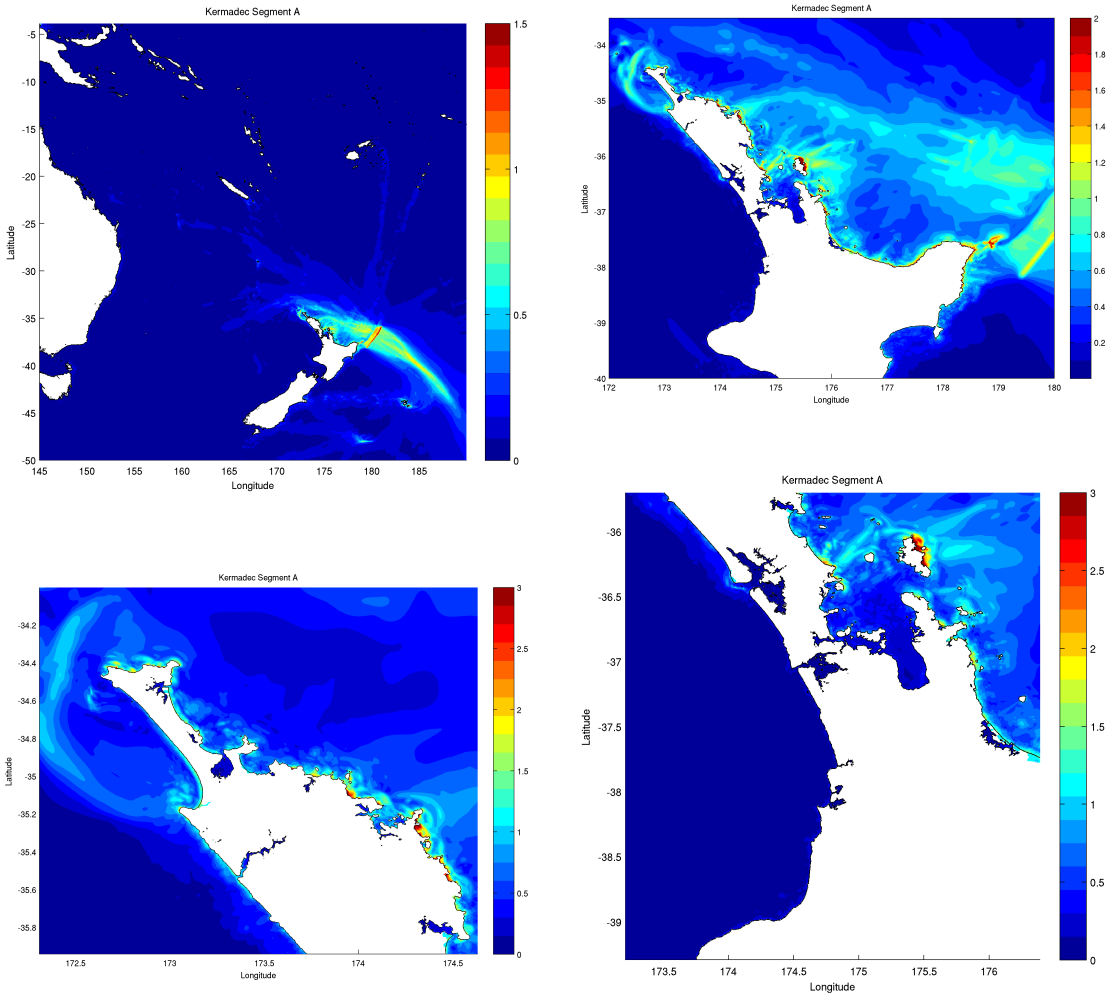

Figure 8: Maximum water level plots (in meters) for scenario 1, Mw 8.5 segment A.

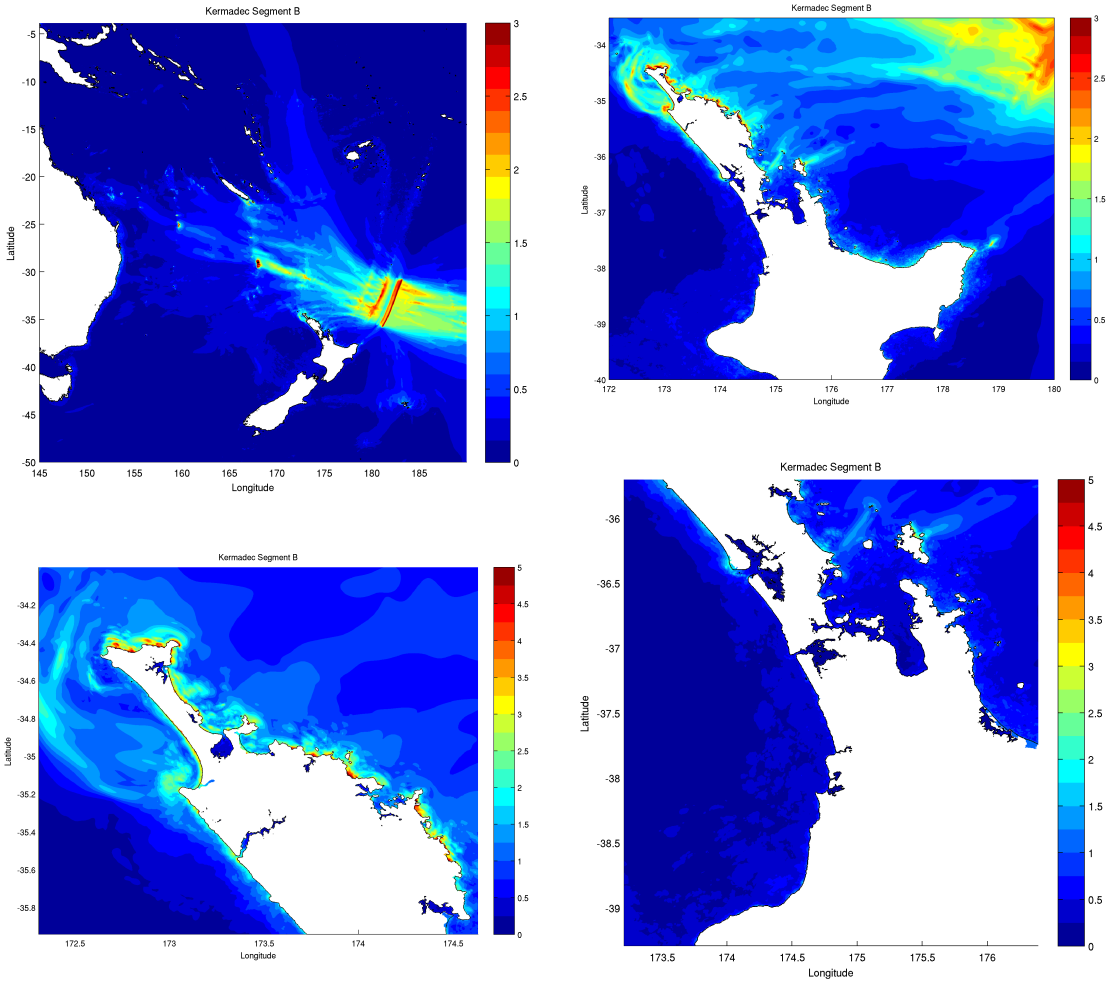

Figure 9: Maximum water level plots (in meters) for scenario 2, Mw 8.9 segment B.

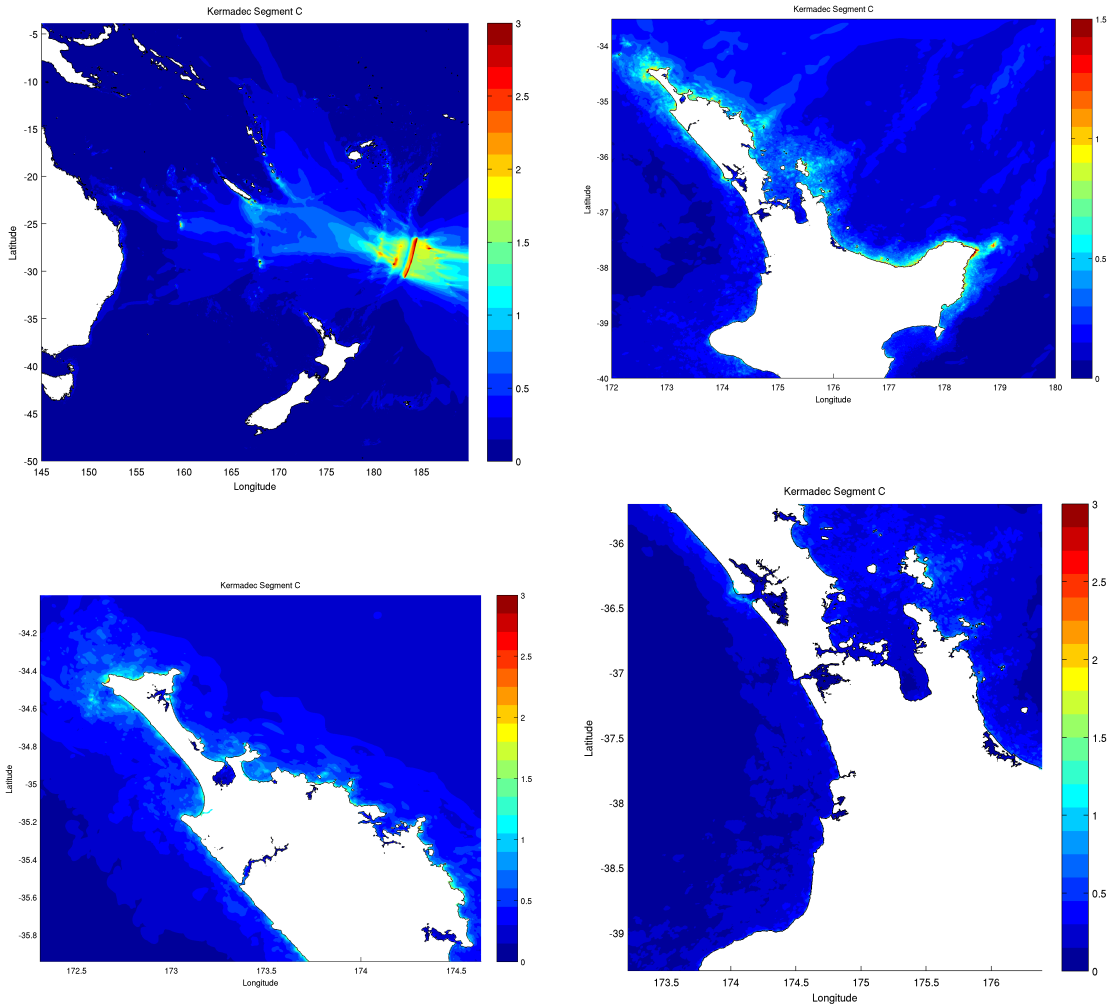

Figure 10: Maximum water level plots (in meters) for scenario 3, Mw 8.8 segment C.

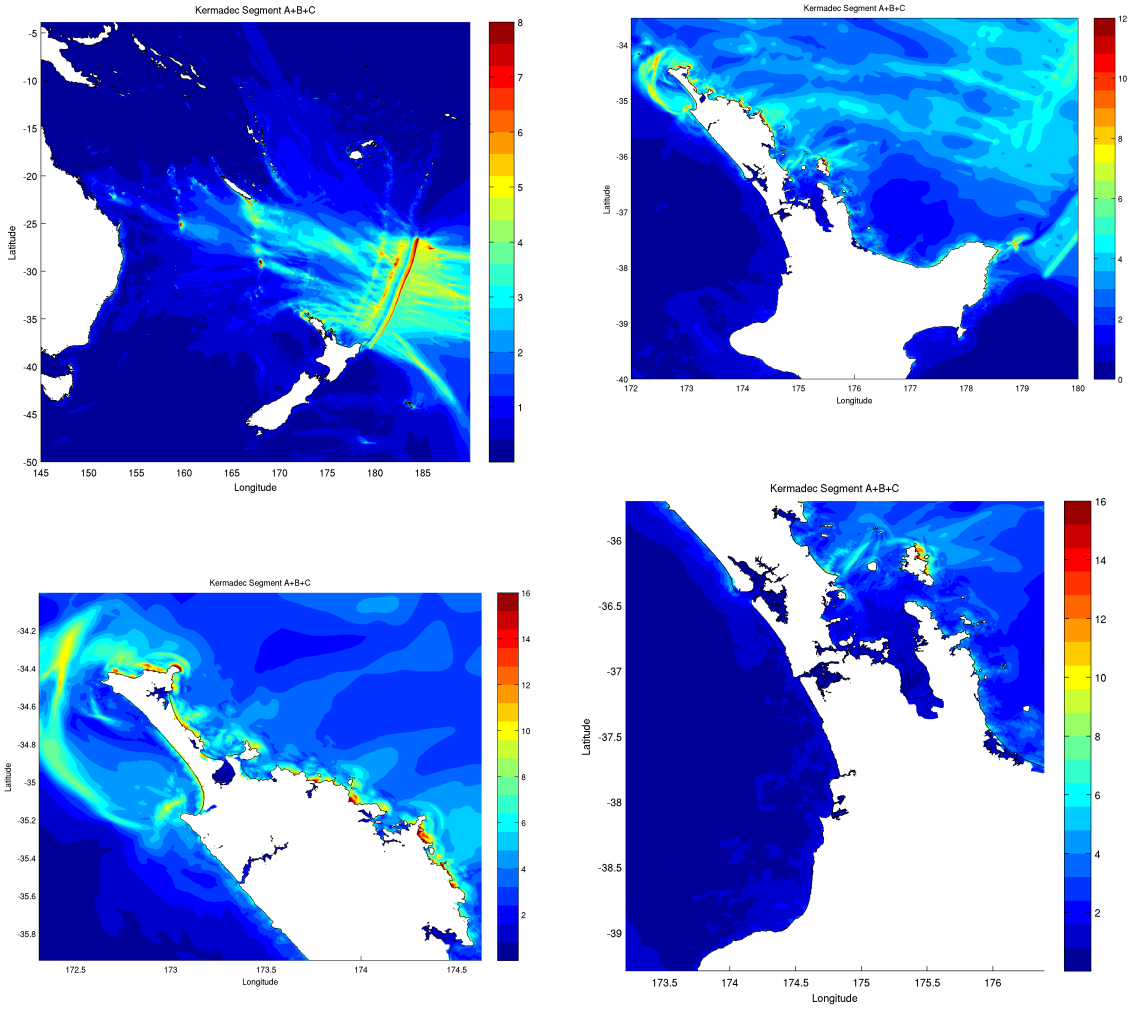

Figure 11: Maximum water level plots (in meters) for scenario 4, Mw 9.4 segments A+B+C.

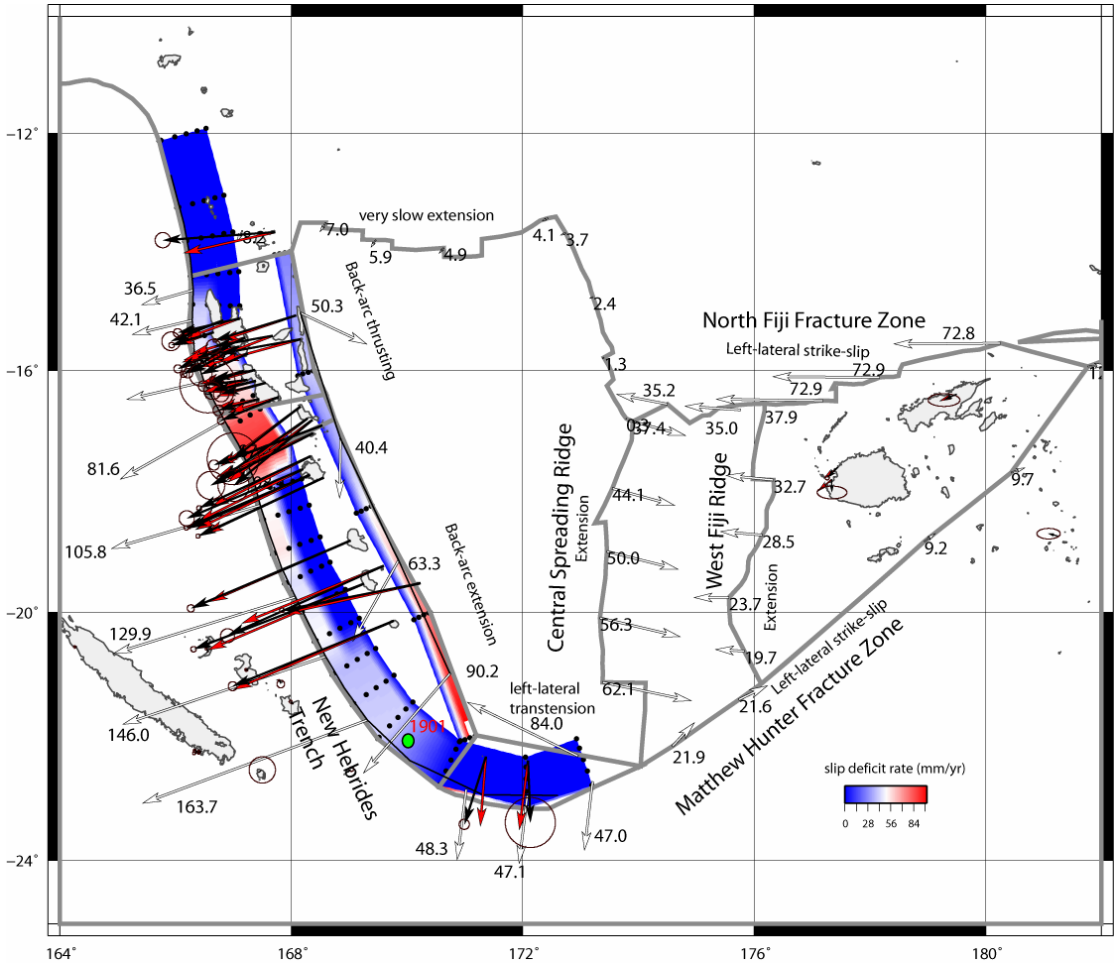

Figure 12: Plate kinematic and fault locking (in terms of slip deficit rate) results from block modelling of earthquake slip vector data and GPS velocities in the Vanuatu/north Fiji Basin region. Black arrows are the observed GPS velocities, while the red arrows are the predicted velocities from best-fitting inversion. White arrows on the boundaries are the long-term relative motion between adjacent blocks (labelled with rates in mm/yr). The green circle shows the location of the 1901 earthquake described in the text.

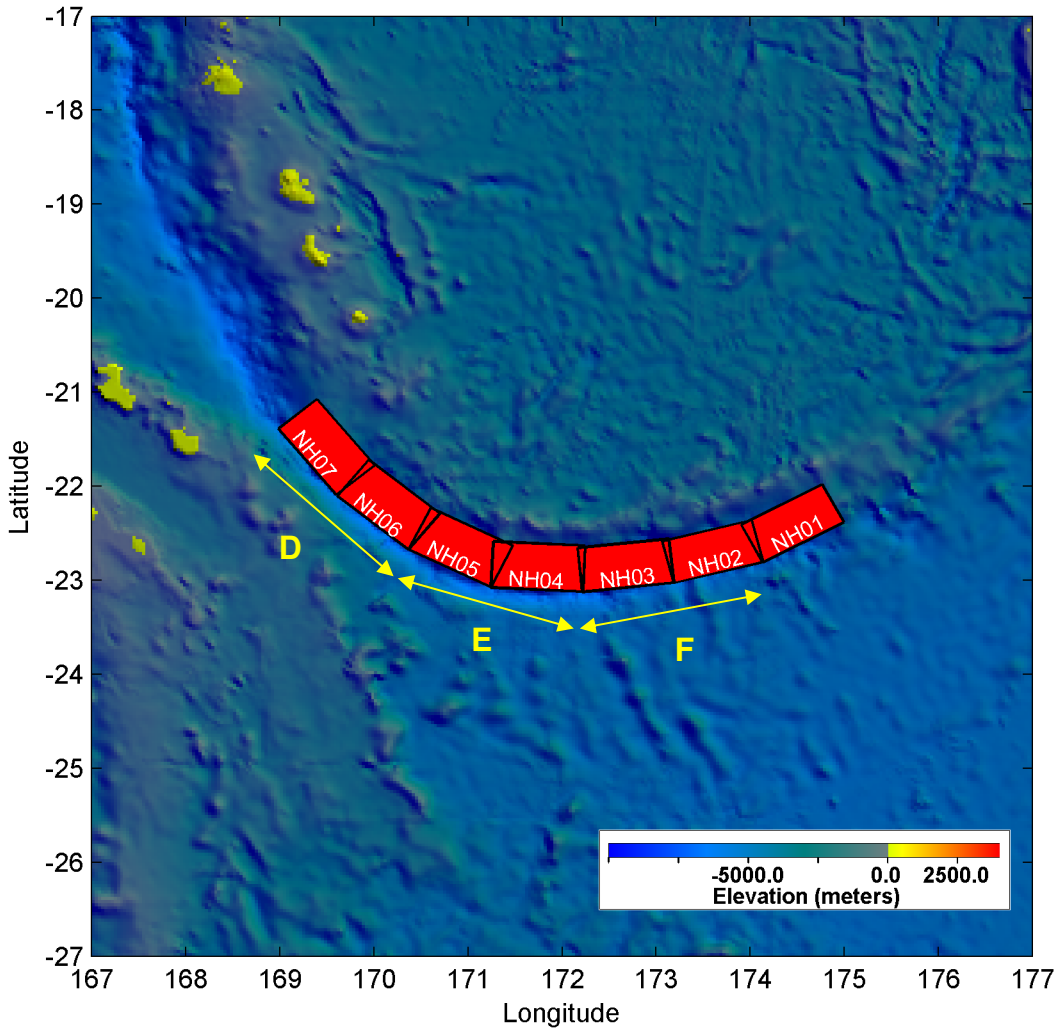

Figure 13: Unit patches of southern New Hebrides subduction interface. D,E and F represent the segmentation used for scenario events.

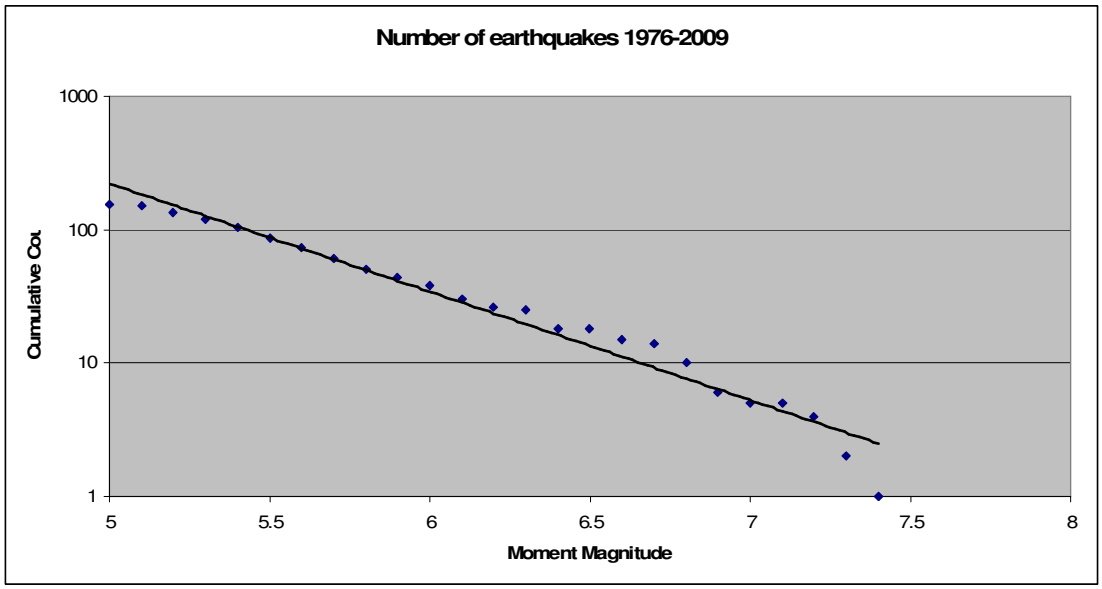

Figure 14. Cumulative number of subduction thrust earthquakes on the south New Hebrides Arc, for the period 1976-2009 inclusive, exceeding a given moment magnitude.

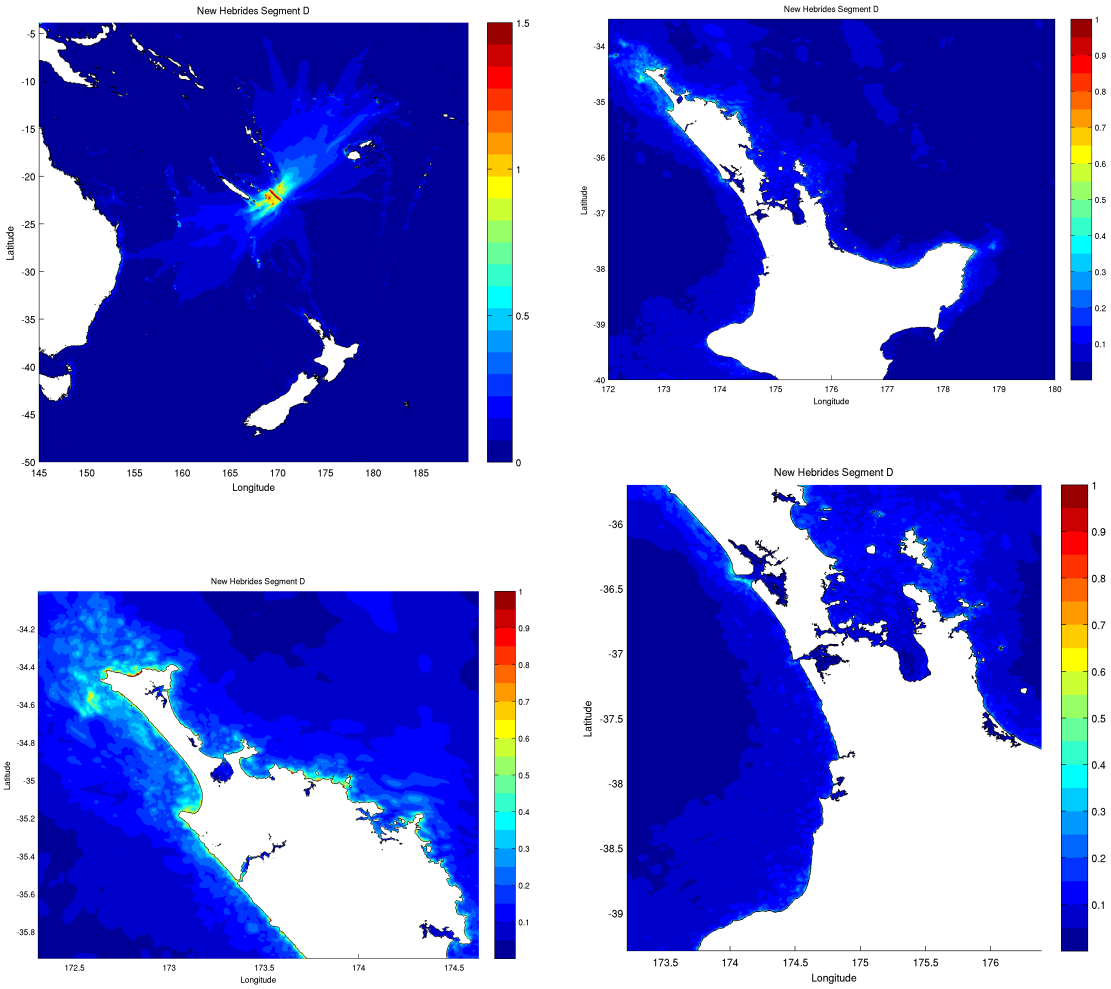

Figure 15: Maximum water level plots (in meters) for scenario 5, Mw 8.15 segment D

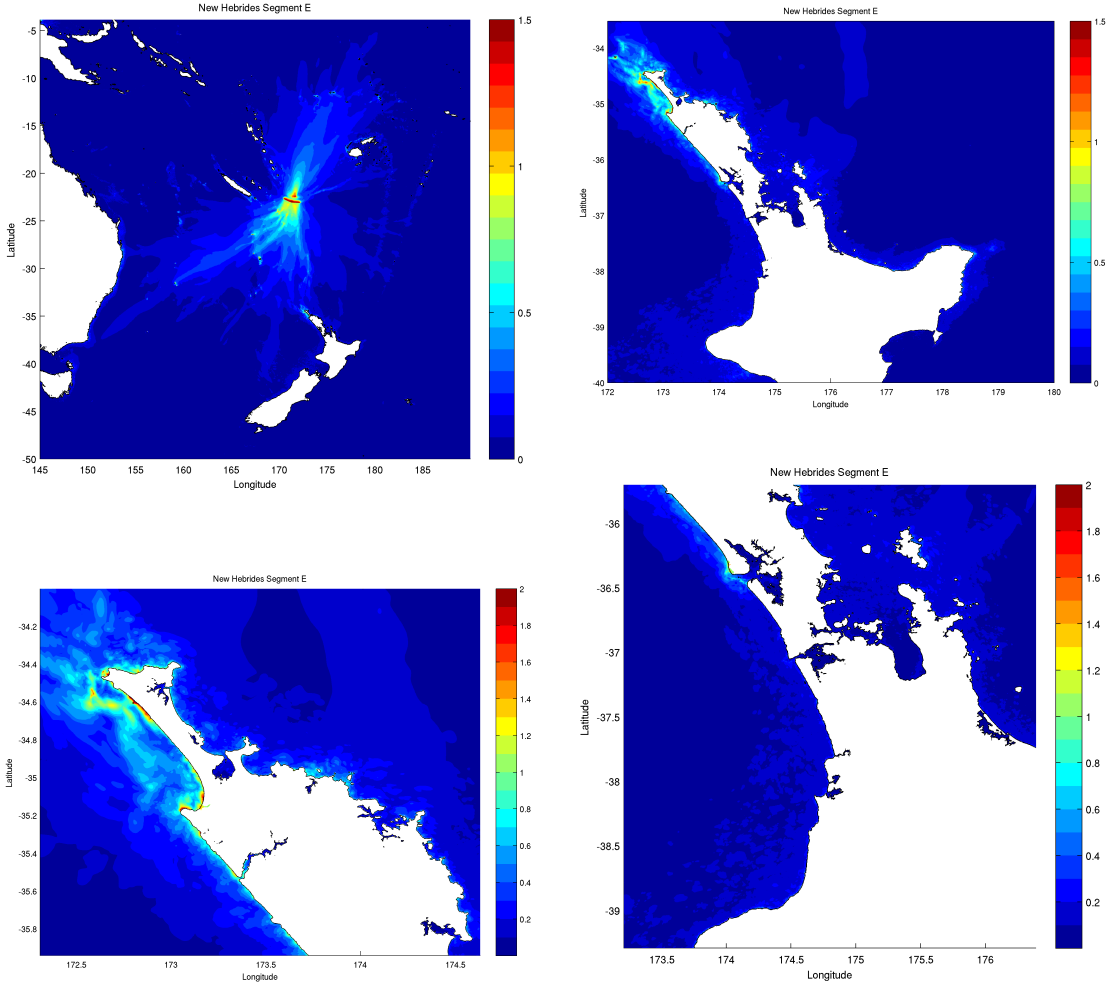

Figure 16: Maximum water level plots (in meters) for scenario 6, Mw 8.15 segment E

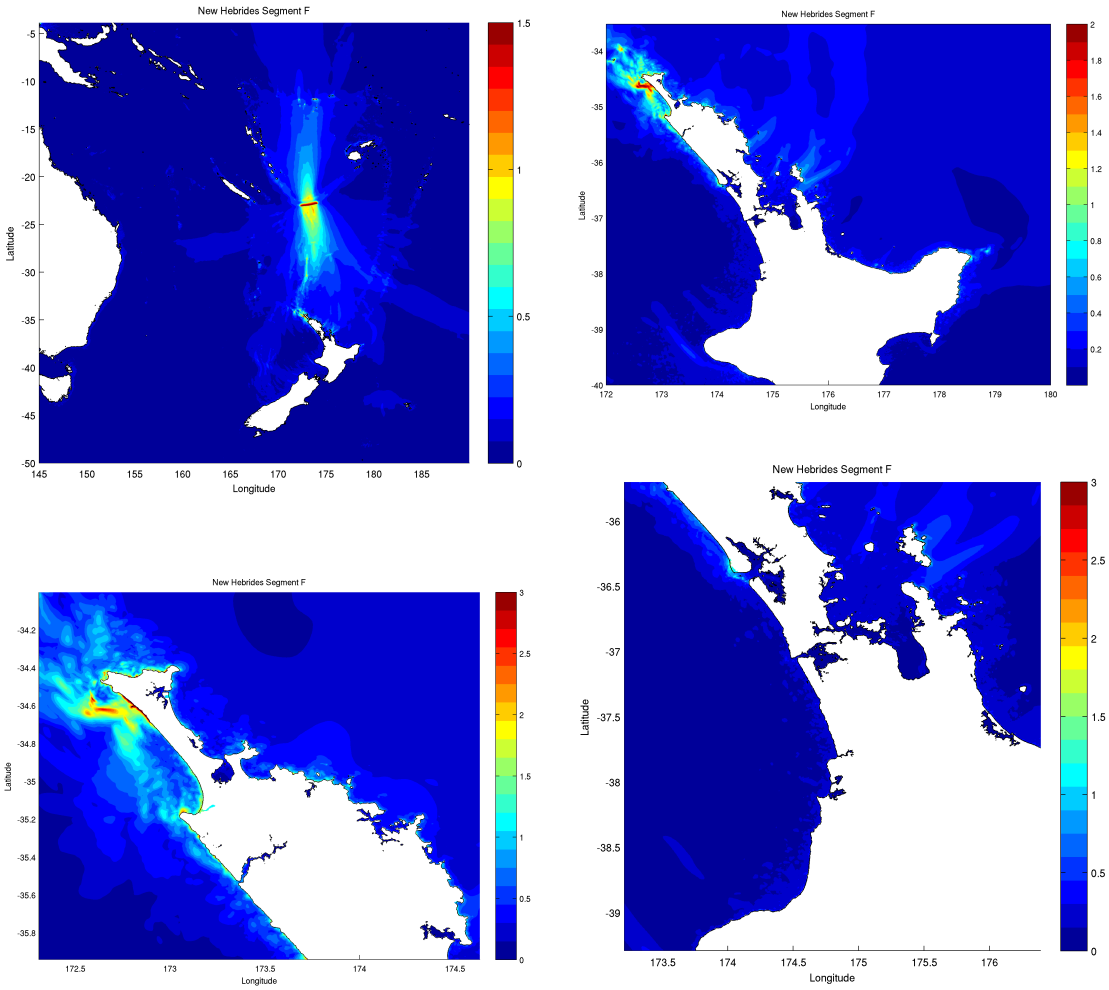

Figure 17: Maximum water level plots (in meters) for scenario 7, Mw 8.15 segment F

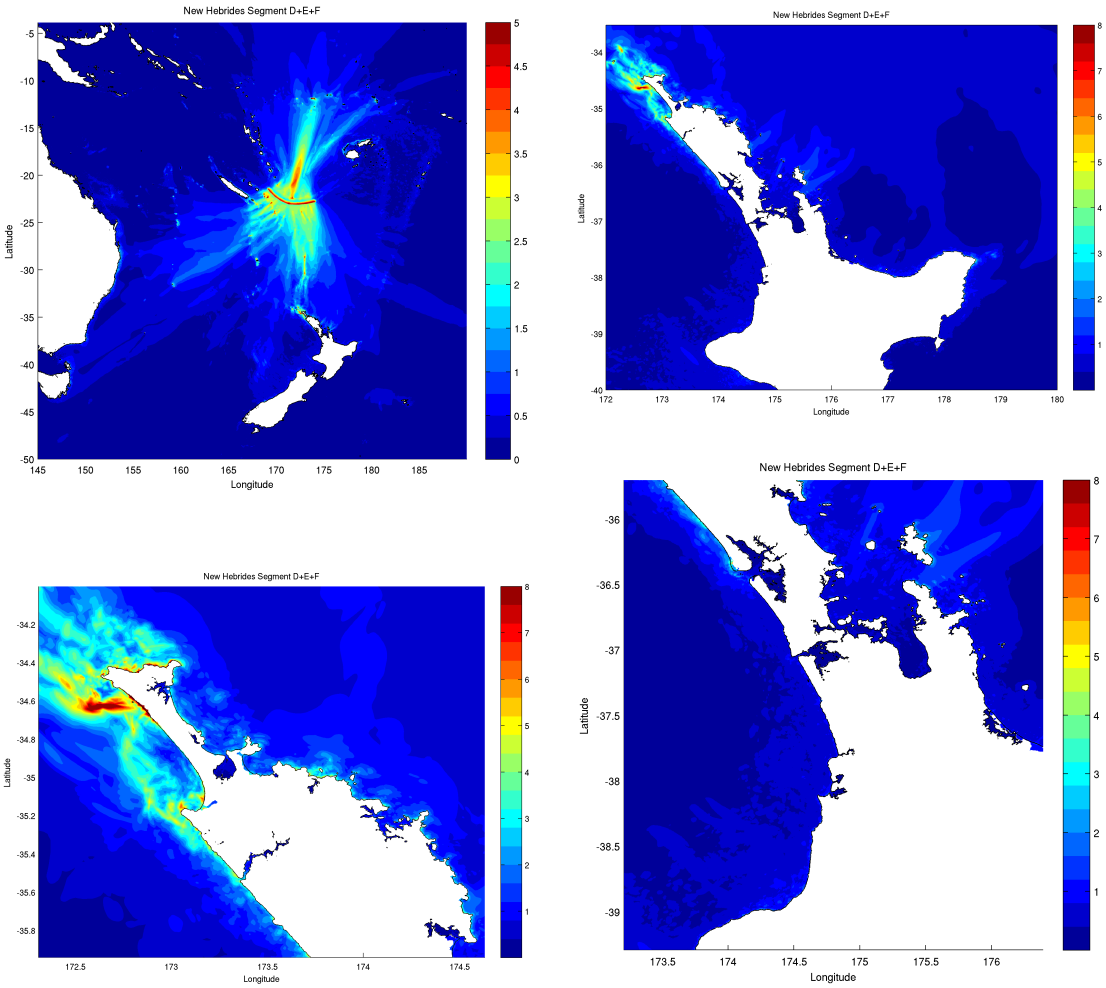

Figure 18: Maximum water level plots (in meters) for scenario 8, Mw 8.8 segments D+E+F

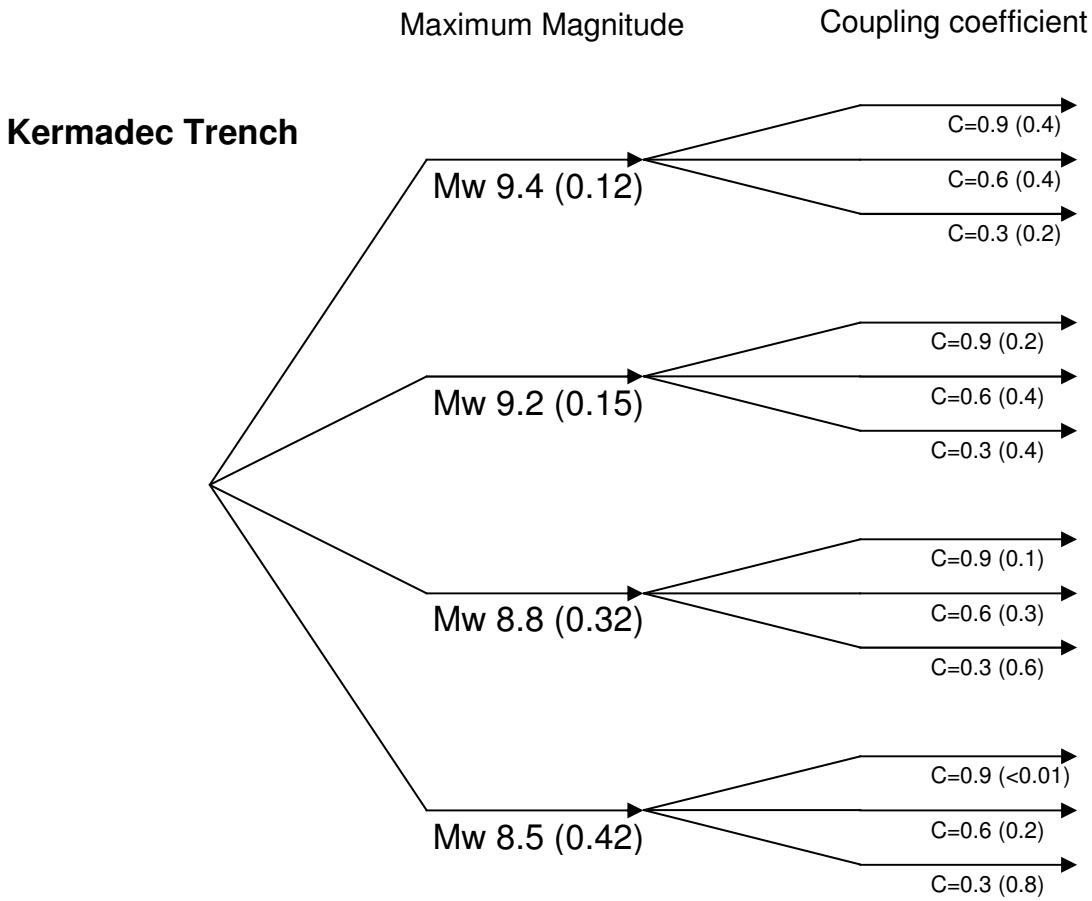

Figure A1: Kermadec Trench logic tree

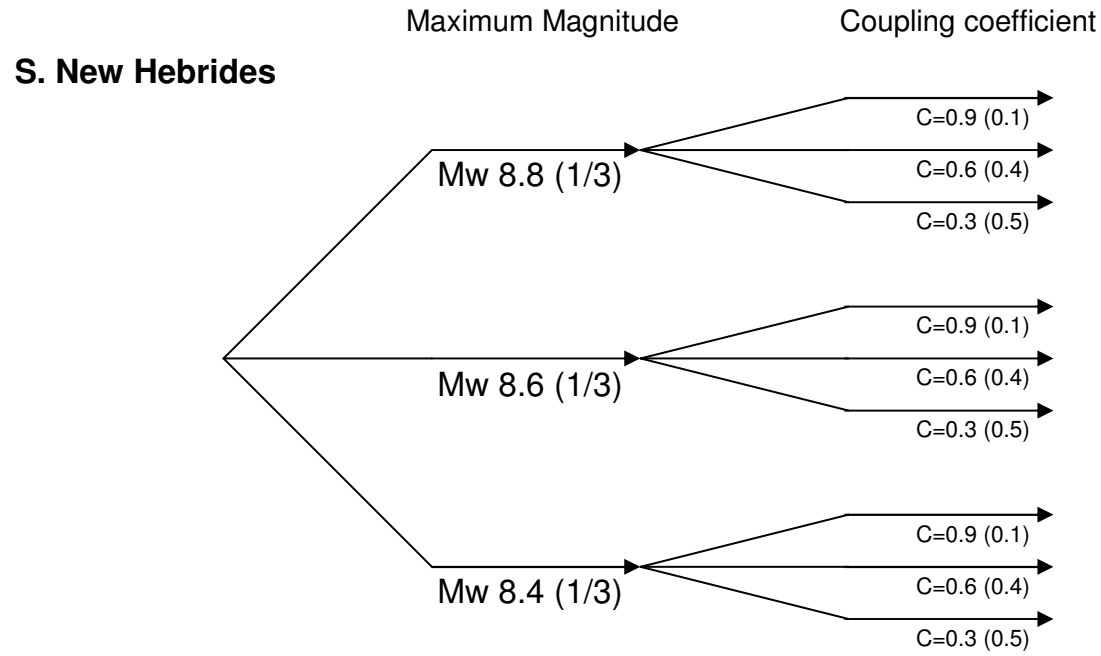

Figure A2: Southern New Hebrides logic tree

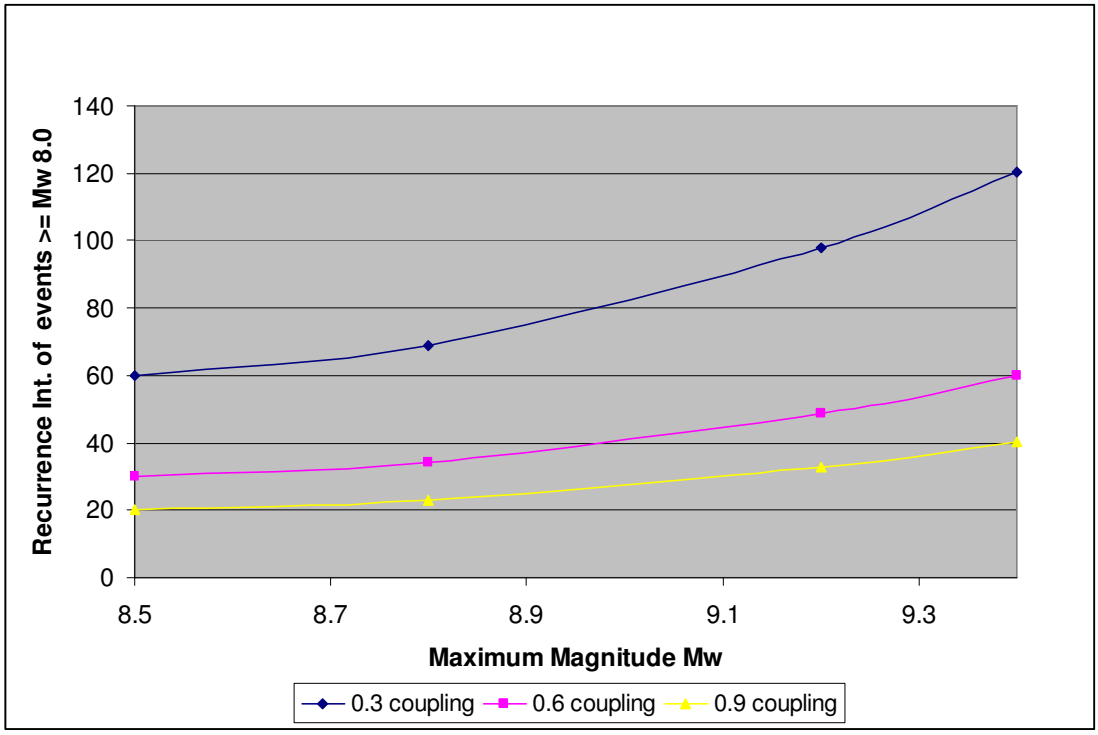

Figure A3: Average Recurrence Interval between earthquakes of Mw ≥ 8.0 plotted as a function of maximum magnitude and seismic coupling coefficient, assuming a truncated Guttenberg-Richter distribution and 72 mm/yr convergence rate.